bioRxiv preprint doi: https://doi.org/10.1101/2025.02.14.638315; this version posted February 15, 2025. The copyright holder for this preprint (which was not certified by peer review) is the author/funder, who has granted bioRxiv a license to display the preprint in perpetuity. It is made available under aCC-BY-NC-ND 4.0 International license.

Forward genetic screen in zebrafish identifies new fungal regulators that limit host-protective *Candida*-innate immune interaction

Bailey A. Blair[1,2], Emma Bragdon[1], Gursimran Dhillon[1], Nnamdi Baker[1], Lena Stasiak[1], Mya Muthig[1], Pedro Miramon[3], Michael C. Lorenz[3], Robert T. Wheeler[1,2,*]

[1]Department of Molecular & Biomedical Sciences, University of Maine, Orono, ME 04469

[2]Graduate School of Biomedical Sciences and Engineering, University of Maine, Orono, ME 04469

[3]Department of Microbiology and Molecular Genetics, McGovern Medical School, The University of Texas Health Science Center at Houston, Houston, USA.

[*]Correspondence:

Robert T. Wheeler

5735 Hitchner Hall

Orono, ME 04469

robert.wheeler1@maine.edu

207-581-2890

Running title: *Candida* evasion of phagocytes

bioRxiv preprint doi: https://doi.org/10.1101/2025.02.14.638315; this version posted February 15, 2025. The copyright holder for this preprint (which was not certified by peer review) is the author/funder, who has granted bioRxiv a license to display the preprint in perpetuity. It is made available under aCC-BY-NC-ND 4.0 International license.

Abstract

Candida is one of the most frequent causes of bloodstream infections, and our first line of defense against these invasive infections is the innate immune system. The early immune response is critical in controlling *C. albicans* infection, but *C. albicans* has several strategies to evade host immune attack. Phagocytosis of *C. albicans* blocks hyphal growth, limiting host damage and virulence, but how *C. albicans* limits early recruitment and phagocytosis in vertebrate infection is poorly understood. To study innate immune evasion by intravital imaging, we utilized the transparent larval zebrafish infection model to screen 131 *C. albicans* mutants for altered virulence and phagocyte response. Infections with each of seven hypovirulent mutants led to altered phagocyte recruitment and/or phagocytosis, falling into four categories. Of particular interest among these is *NMD5*, a predicted β-importin and newly-identified virulence factor. The *nmd5*Δ/Δ mutant fails to limit phagocytosis and its virulence defects are eliminated when phagocyte activity is compromised, suggesting that its role in virulence is limited to immune evasion. These quantitative intravital imaging experiments are the first to document altered *Candida*-phagocyte interactions for several additional mutants, and clearly distinguish recruitment from phagocytic uptake, suggesting that *Candida* modulates both events. This initial large-scale screen of individual *C. albicans* mutants in a vertebrate, coupled with high-resolution imaging of *Candida*-phagocyte interactions, provides a more nuanced view of how diverse mutations can lead to more effective phagocytosis, a key immune process which blocks germination and drives anti-fungal immunity.

bioRxiv preprint doi: https://doi.org/10.1101/2025.02.14.638315; this version posted February 15, 2025. The copyright holder for this preprint (which was not certified by peer review) is the author/funder, who has granted bioRxiv a license to display the preprint in perpetuity. It is made available under aCC-BY-NC-ND 4.0 International license.

Importance

Candida albicans is part of the human microbial community and is a dangerous opportunistic pathogen, able to prevent its elimination by the host immune system. Although *Candida* avoids immune attack through several strategies, we still understand little about how it regulates when immune phagocytes get recruited to the infection site and when they engulf fungal cells. We tested over 130 selected *Candida* mutants for their ability to cause lethal infection and found several avirulent mutants which provoked altered innate immune responses, resulting in lower overall inflammation and greater host survival. Of particular interest is *NMD5*, which acts to limit fungal phagocytosis and is predicted to regulate the activity of stress-associated transcription factors. Our high-content screening was enabled by modeling *Candida* infection in transparent vertebrate zebrafish larva. Our findings help us understand how *Candida* survives immune attack during commensal and pathogenic growth, and may eventually inform new strategies for controlling disease.

bioRxiv preprint doi: https://doi.org/10.1101/2025.02.14.638315; this version posted February 15, 2025. The copyright holder for this preprint (which was not certified by peer review) is the author/funder, who has granted bioRxiv a license to display the preprint in perpetuity. It is made available under aCC-BY-NC-ND 4.0 International license.

Introduction

Candida albicans is the one of most common bloodstream infections in the U.S. causing approximately 25,000 cases annually (CDC). *C. albicans* can normally be found as a commensal in the gastrointestinal tract, mouth, skin, or vagina in up to 70% of the population (1-3). While *C. albicans* is found in healthy individuals it can also cause infections ranging from superficial mucosal infections such as vulvovaginal candidiasis and oropharyngeal candidiasis, to lethal systemic infections with attributable mortality rates of approximately 25% (4, 5). The host immune response is tasked with protecting individuals from these infections with the innate immune system being of special importance in fighting systemic *Candida* infections. In turn, *C. albicans* employs many mechanisms to subvert the actions of the host immune attack (6-14). While we understand some of how *C. albicans* can evade host immune responses *in vitro*, we still know little about this during vertebrate infection.

The innate immune response is the first line of defense against *C. albicans*, and is critical in controlling and preventing systemic candidiasis (15-19). This is highlighted by the fact that patients with neutropenia are more susceptible to invasive *Candida* infections, and mice with macrophage defects survive experimental systemic infection poorly. Phagocytes get to the infection site by following cytokine and chemokine gradients and presumably identify fungal cells for ingestion using fungal-derived chemoattractants (17, 18, 20). While phagocytes play crucial roles, other innate immune cells such as epithelial cells, microglia, natural killer cells and innate lymphocytes also play important roles (18, 21). Cytokines and chemokines, which bring phagocytes to the infection site, simultaneously activate them and induce their differentiation. Once there, phagocytes must locate fungal cells by soluble cues, recognize the foreign microbial cells based on surface patterns and opsonins, and initiate phagocytosis.

bioRxiv preprint doi: https://doi.org/10.1101/2025.02.14.638315; this version posted February 15, 2025. The copyright holder for this preprint (which was not certified by peer review) is the author/funder, who has granted bioRxiv a license to display the preprint in perpetuity. It is made available under aCC-BY-NC-ND 4.0 International license.

Immune cells such as phagocytes recognize pathogen associated molecular patters (PAMPs) in *C. albicans* cell wall, but *C. albicans* is able to shield them from immune cells behind a layer of mannosylated proteins of the outer cell wall (9). Macrophages and neutrophils are the main effector cells against *C. albicans* and employ many strategies to kill *C. albicans.* These cells are able to phagocytose *C. albicans* yeast as well as short hyphae, produce antimicrobial peptides, reactive oxygen species, and extracellular traps to combat *C. albicans* (8, 13, 14, 22). Not only can *C. albicans* shield its cell wall PAMPs from these cells, but once taken up by a phagocyte *C. albicans* can survive by preventing the fusion of the phagosome with the lysosome, alkanizing the acidic environment of the phagolysosome, producing catalase and superoxide dismutase to counteract ROS, and upregulating DNA repair systems and heat shock proteins to counteract damage caused to DNA and proteins (23, 24). In addition, *C. albicans* has also been seen to escape from host cells such as macrophages by inducing pyroptosis; or also, although rare, vomocytosis (25) (23). These mechanisms were initially described *in vitro*, yet we still do not fully understand which mechanisms play critical roles during infection or which fungal pathways mediate these activities

The larval zebrafish provides a unique model that is well-suited to investigate the interactions between *C. albicans* and the vertebrate innate immune response (26-28). The transparency and availability of many transgenic lines permits quantitative imaging of the immune response to *C. albicans* infection in the context of a live host. Furthermore, the small size and fertility of zebrafish enables cost-effective moderate- to high-throughput screening in a vertebrate model. Previous results suggest that the early phagocyte response is critical to survive a *C. albicans* hindbrain ventricle infection (29, 30). Evidence from the larval zebrafish also suggest that *C. albicans* has the ability to limit this response be reducing the recruitment of

bioRxiv preprint doi: https://doi.org/10.1101/2025.02.14.638315; this version posted February 15, 2025. The copyright holder for this preprint (which was not certified by peer review) is the author/funder, who has granted bioRxiv a license to display the preprint in perpetuity. It is made available under aCC-BY-NC-ND 4.0 International license.

phagocytes to the infection site (30). This ability to limit phagocyte recruitment was observed for a WT *C. albicans* strain, but not a yeast locked strain, suggesting this response may be regulated with the yeast to hyphal transition.

We sought to identify new *C. albicans* factors playing a role in limiting early phagocyte responses by leveraging the transparent zebrafish infection model. Since virulence is linked to early phagocytic efficiency, we screened 131 engineered *C. albicans* mutants for virulence defects in the larval zebrafish hindbrain infection model. Since there may be links between evasion of phagocyte recruitment and the yeast-to-hyphal transition, we chose a set of mutants that had been characterized in a previous high-throughput pooled screen as having either an infectivity defect only or a morphogenesis defect only (31). Since little is known about soluble chemoattractants secreted by *Candida*, we also included single mutants from groups of genes that code for potential secreted proteins such as secreted aspartyl proteases and lipases. Mutations that were associated with hypovirulence and could be faithfully complemented were then screened for multiple phagocyte recruitment and phagocytosis phenotypes during early infection. Several genes previously known to alter morphology and/or virulence were found to limit early phagocytosis of *Candida*, a previously unknown function of these genes. Strikingly, the predicted karyopherin *NMD5* lost its virulence defect when the host was immunosuppressed in any of three ways—suggesting that its role in virulence is largely confined to limiting early phagocyte recruitment and phagocytosis. These results expand our understanding of how *Candida* virulence genes mediate pathogenesis through limiting the early innate immune response.

bioRxiv preprint doi: https://doi.org/10.1101/2025.02.14.638315; this version posted February 15, 2025. The copyright holder for this preprint (which was not certified by peer review) is the author/funder, who has granted bioRxiv a license to display the preprint in perpetuity. It is made available under aCC-BY-NC-ND 4.0 International license.

Results

Forward genetic screen for altered fungal immune evasion based on loss of virulence

C. albicans is known to limit immune recruitment and phagocytosis during infection, although morphological switching can regulate phagocyte recruitment, few molecular details are known about how this occurs (30, 32, 33). The zebrafish hindbrain infection model provides a useful *in vivo* system to intravitally image early fungal and host dynamics, and has identified a close correlation between early phagocyte-mediated fungal containment and overall survival (29, 30, 33). We leveraged these advantages to screen individual *C. albicans* mutants for virulence and phagocytosis defects, with an initial screen for hypovirulence and a secondary screen for altered fungal-phagocyte interaction.

We used a small number of mutants to define infection parameters and enable high-throughput screening; these mutants have normal *in vitro* competitive fitness, were present in our strain collections, and are predicted to have cell wall defects (*mnn15*Δ/Δ, *mnt1*Δ/Δ), known to have filamentous growth defects or altered interaction with phagocytes *in vitro* (*mad2*Δ/Δ, *ece1*Δ/Δ, *pra1*Δ/Δ), and/or hypovirulence in murine models (Table S1) (34-37). In initial virulence tests, two mutant strains were tested along with controls and at least 3 biologically independent experiments were performed with approximately 50 fish infected per mutant (Fig. 1A). Inoculums were counted by fluorescence microscopy to ensure they received the correct amount of *Candida* (10-25 fungal cells), then larvae were followed for survival for three days relative to the SN250 wildtype (Fig. 1B). Three of the nine strains tested had significantly reduced (*ssu81*Δ/Δ & *mad2*Δ/Δ) or abolished virulence *rbt1*Δ/Δ$^{968\text{-}2166}$ (Fig. 1C). We then used the average and standard deviation of 72 hours post infection (hpi) survival for wildtype-infected fish to determine z-score cutoffs for subsequent experiments, to exclude data in which wildtype-

bioRxiv preprint doi: https://doi.org/10.1101/2025.02.14.638315; this version posted February 15, 2025. The copyright holder for this preprint (which was not certified by peer review) is the author/funder, who has granted bioRxiv a license to display the preprint in perpetuity. It is made available under aCC-BY-NC-ND 4.0 International license.

131 infected survival was out of range (average +/- 2.5 SD [20 - 80% survival]). In addition, we
132 quantified host-pathogen interactions by confocal microscopy at 4-6 hpi, scoring fungal cells as
133 intra- versus extra-cellular based on a combination of Calcofluor white staining of the inoculum
134 and DIC imaging of host phagocytes (Fig. 1D-insets & 1E). Although this method was limited
135 because only the initial inoculum was fluorescently stained and phagocytes were not fluorescent,
136 there was a consistent trend for increased fungal phagocytosis of *mad2*Δ/Δ compared to the
137 control SN250 (Fig. 1E, Table S2, p=0.009, effect size = 0.90; large). The *rbt4*Δ/Δ mutant was
138 phagocytosed significantly less efficiently (p=0.029, effect size =0.55; large), but was not
139 pursued further because the lower phagocytosis was not associated with altered survival (Fig.
140 1C). Interestingly, *mad2*Δ/Δ was also one of three strains with significantly reduced virulence
141 (Fig. 1B-C). The other two hypovirulent mutants failed later validation steps—*rbt1*Δ/Δ$^{968\text{-}2166}$
142 failed at the complementation step and *ssu81*Δ/Δ failed when the second isolate was tested.
143 Although morphological quantification of the fungi was not possible because only the inoculum
144 was labeled, and the inoculum was all yeast cells for all strains, there were no qualitative
145 differences noted in the amount of filamentous growth (as visualized by brightfield microscopy)
146 between SN250 and any of the mutant strains.

147 A total of 131 mutant *C. albicans* strains with expected deficiencies in predicted secreted
148 factors, hyphal growth, or virulence were then selected for screening (Table S1), based on their
149 phenotypes observed in previous screens (31). One group of strains (the Morphology category)
150 were selected for a published defect in hyphal growth on Spider medium but no defect in
151 virulence, as we hypothesized that these mutants might disrupt the co-regulation of immune
152 evasion mechanisms with the yeast-to-hyphal transition (10). While these strains have a
153 morphogenesis defect on Spider plates, defects in filamentous growth are often very dependent

bioRxiv preprint doi: https://doi.org/10.1101/2025.02.14.638315; this version posted February 15, 2025. The copyright holder for this preprint (which was not certified by peer review) is the author/funder, who has granted bioRxiv a license to display the preprint in perpetuity. It is made available under aCC-BY-NC-ND 4.0 International license.

on the environmental context and strain, and therefore may or may not have a filamentous growth defect in the zebrafish hindbrain (38-40). A complementary set of strains (the Infectivity category) had a competitive defect in pooled mouse infection but no morphogenesis defect on Spider agar; we reasoned these strains may be cleared more effectively by the host immune response even if they are not defective in filamentous growth. This included 69 mutants that had a morphogenesis defect on Spider agar but no pooled virulence defect, 41 that had an infectivity defect in pooled infection but no Spider morphogenesis defect, and one had both defects. The final category (Secreted-Predicted) included 20 genes encoding predicted secreted peptides—including lipases, proteases and other genes annotated as potentially secreted—but the mutants had no Spider agar morphogenesis or pooled virulence defect (31) (Table S1).

In this primary screen we chose to facilitate high-throughput screening for cell-autonomous virulence defects, so inoculums were not counted and no replicates were performed. Virulence testing revealed several mutants with greatly reduced virulence, as measured by z-score (based on deviance from the mean for WT infection, see Materials and Methods). Seventeen had a fish survival z-score > 3, while 27 had a z-score between 2 and 3 (Fig. 2). Of the 41 strains in the Infectivity category, 6 of these had a z-score >3, with another 6 between z-scores of 2 and 3. Out of the 70 in the Morphogenesis category, 11 had z-score > 3, with another 16 between 2 and 3. In addition, 4 genes from the secreted aspartyl protease (SAP) family of genes had z-scores between 2 and 3. As these fish were not screened to ensure the correct number of *C. albicans* injected (10-25 fungal cells), we first retested hypovirulent strains with z-scores > 3 with an added step of screening for inoculum per fish. On retest, both independent isolates from the Noble library were tested and strains were genotyped to confirm the correct gene deletion. After retesting, this led to a total of 10 mutants with reproducible hypovirulence:

bioRxiv preprint doi: https://doi.org/10.1101/2025.02.14.638315; this version posted February 15, 2025. The copyright holder for this preprint (which was not certified by peer review) is the author/funder, who has granted bioRxiv a license to display the preprint in perpetuity. It is made available under aCC-BY-NC-ND 4.0 International license.

177 *rbt1*Δ/Δ$^{968\text{-}2166}$, *orf19.5547*Δ/Δ, *pep8*Δ/Δ, *cht2*Δ/Δ, *apm1*Δ/Δ, *rim101*Δ/Δ, *brg1*Δ/Δ, *nmd5*Δ/Δ,
178 *mad2*Δ/Δ, and *cek1*Δ/Δ (Table S1). Hypovirulent strains were then complemented to assess if
179 complementation restored virulence. When available, *in vitro* phenotypes (e.g. morphogenesis
180 defect on Spider media) were also used to assess functional complementation of strains prior to
181 assessing virulence in hindbrain infection. Complementation successfully restored at least some
182 virulence to *brg1*Δ/Δ, *pep8*Δ/Δ, *nmd5*Δ/Δ, *rim101*Δ/Δ, *cek1*Δ/Δ, *apm1*Δ/Δ, and *mad2*Δ/Δ mutants
183 (Fig. 3). It also partially restored *in vitro* filamentous growth and pH-dependent filamentation
184 phenotypes for *brg1*Δ/Δ, *pep8*Δ/Δ and *rim101*Δ/Δ (Fig. S1). We were not able to generate
185 complemented strains that restored even partial virulence to *cht2*Δ/Δ, *orf19.5547*Δ/Δ, or
186 *rbt1*Δ/Δ$^{968\text{-}2166}$ (Fig. S2A-C). Consistent with the failure to complement the partial ORF deletion
187 in *RBT1*, an independently-created full deletion of *RBT1* in the SN250 background did not cause
188 a virulence defect (Fig. S2D). The failure to complement the virulence defects in these strains
189 with the full-length gene suggests that the virulence defect is due to other, non-targeted, genomic
190 changes sustained during their original construction. Mutants that could be complemented were
191 then transformed with pENO1-iRFP (41) to drive cytosolic expression of a near-infrared
192 fluorescent protein for intravital imaging of infections. At the conclusion of this first part of the
193 screen, we were left with seven mutants whose virulence defects could be at least partially
194 complemented with add-back of a full-length copy of the gene: five in the Morphogenesis class
195 (*brg1*Δ/Δ, *pep8*Δ/Δ, *rim101*Δ/Δ, *apm1*Δ/Δ, and *cek1*Δ/Δ), two in the Infectivity class (*nmd5*Δ/Δ
196 and *mad2*Δ/Δ) and none in the Predicted Secreted class.
197
198 **Altered early phagocyte responses to hypovirulent *Candida* mutants**

bioRxiv preprint doi: https://doi.org/10.1101/2025.02.14.638315; this version posted February 15, 2025. The copyright holder for this preprint (which was not certified by peer review) is the author/funder, who has granted bioRxiv a license to display the preprint in perpetuity. It is made available under aCC-BY-NC-ND 4.0 International license.

Previous work has linked efficient early immune phagocytosis of fungi to enhanced survival (29, 30). To determine if the virulence defects for these mutants were associated with a more effective early immune response, we imaged *Tg(mpeg1:GFP)/(lysC:dsRed)* larvae (green macrophages and red neutrophils) infected with iRFP-expressing *Candida* at 4-6 hpi. From these images, we assessed the number of macrophages and neutrophils responding rapidly to infection as well as their ability to phagocytose *Candida*, as measured by the number of extracellular fungi, percent phagocytosis and the number fungi/recruited phagocyte. We chose these measures to quantify (1) the overall ability of phagocytes to internalize fungi, keep them internalized, and prevent their extracellular proliferation; (2) the relative efficiency of phagocytosis, without consideration of the total number of extracellular cells, indicating the overall capacity of recruited phagocytes to engulf fungi; and (3) the average ability of any given phagocyte at the infection site to engulf fungi, providing an indicator of the activation state of the phagocytes and their ability to identify and engulf fungi.

Overall, we found altered acute immune responses to each of the seven validated hypovirulent mutants, with mutant phenotypes in four groups based on infection site immune cell counts and phagocytosis efficiency at 4-6 hpi (Table 1). Three mutants in Group I (*mad2*Δ/Δ, *rim101*Δ/Δ and *brg1*Δ/Δ) were phagocytosed more effectively and there were lower phagocyte numbers at the infection site at 4-6 hpi. Two mutants in Group II (*pep8*Δ/Δ and *apm1*Δ/Δ) had unchanged phagocytosis efficiency and fewer immune cells. One (Group III; *nmd5*Δ/Δ) had greater phagocytosis with an unchanged phagocyte number and one (Group IV; *cek1*Δ/Δ) had increased phagocytosis and an increased phagocyte count. The phenotypic scoring is described below in more detail.

bioRxiv preprint doi: https://doi.org/10.1101/2025.02.14.638315; this version posted February 15, 2025. The copyright holder for this preprint (which was not certified by peer review) is the author/funder, who has granted bioRxiv a license to display the preprint in perpetuity. It is made available under aCC-BY-NC-ND 4.0 International license.

Mutants in Groups I, II and IV had altered numbers of phagocytes at the infection site at 4-6 hpi, as evidenced by comparisons with wildtype infections (Fig. 4; p-values and effect sizes summarized in Table 1 and detailed in Table S3; see Materials & Methods). Infections with the *cek1*Δ/Δ mutant elicited a higher number of total phagocytes and macrophages (p-values 0.13, 0.14; effect sizes moderate 0.43, 0.41). In contrast, there was a lower number of macrophages at the infection site in *brg1*Δ/Δ and *pep8*Δ/Δ infections (p-values 0.01, 0.10; effect sizes large, 0.69, or moderate, 0.47) and a lower number of neutrophils in *mad2*Δ/Δ, *rim101*Δ/Δ and *pep8*Δ/Δ infections (p-values 0.066, 0.113, 0.046; effect sizes moderate, 0.44, 0.45, or large, 0.59). The small number of neutrophils present early during infection (often zero) suggests that they usually play a limited role early on, so differential neutrophil recruitment likely has more muted biological consequences. Taken together, these data suggest that there is overall decreased phagocyte recruitment to infections with the Group I (*mad2*Δ/Δ, *rim101*Δ/Δ, *brg1*Δ/Δ) and Group II (*pep8*Δ/Δ and *apm1*Δ/Δ) mutants, and overall increased phagocyte recruitment to *cek1*Δ/Δ (Group IV).

Table 1: Mutants grouped by altered innate immune response

GROUP I				GROUP II			GROUP III		GROUP IV		Phenotype
	rim101 Δ/Δ	*brg1* Δ/Δ	*mad2* Δ/Δ		*pep8* Δ/Δ	*apm1* Δ/Δ		*nmd5* Δ/Δ		*cek1* Δ/Δ	
Fewer immune cells at 4-6 hpi	Down		Down	Fewer immune cells at 4-6 hpi	**Down**		Unchanged immune cells at 4-6 hpi		More immune cells at 4-6 hpi		Neutrophil number
		Down			Down	Down				Up	Macrophage number
	Down		Down		Down	Down				Up	Total phagocyte number
Better phagocytosis and containment	**Down**		**Down**	Unchanged phagocytosis and containment			Better phagocytosis and containment	**Down**	Better phagocytosis and containment	**Down**	Number fungi extracellular
	Up							**Up**		Up	Percent fungal internalization
		Up	Up					Up			Number internalized per phagocyte

Regular text: 0.2<p<0.05	Shaded lightly: Moderate Effect	Green: Decreased relative to WT
Bold: p<0.05	Shaded heavily: Strong Effect	Red: Increased relative to WT

The ability of phagocytes to engulf fungi—and thereby limit filamentous growth and contain the infection—within the first few hours is associated closely with overall survival of a wildtype infection (29, 30). Mutants in Groups I, III and IV had an overall increase in the ability

bioRxiv preprint doi: https://doi.org/10.1101/2025.02.14.638315; this version posted February 15, 2025. The copyright holder for this preprint (which was not certified by peer review) is the author/funder, who has granted bioRxiv a license to display the preprint in perpetuity. It is made available under aCC-BY-NC-ND 4.0 International license.

of phagocytes to internalize fungi. Zebrafish infected with *nmd5*Δ/Δ (Group III) were more effective at each of these measures of fungal internalization (Table 1; Table S3; Fig. 5), with a higher percent internalization (p-value 0.009; large effect size 0.69) and number of fungi per phagocyte (p-value 0.05; large effect size 0.55) and a lower number of extracellular fungi (p-value 0.02; large effect size 0.65). Fish infected with Group I and IV mutants (*mad2*Δ/Δ, *rim101*Δ/Δ, *brg1*Δ/Δ, and *cek1*Δ/Δ) also exhibited at least one measure of increased fungal phagocytosis with at least a moderate effect size (Table 1; Table S3; Fig. 5). Overall, the phagocyte response was able to internalize each of the hypovirulent mutants at least as well as the wildtype strain in the first 4-6 hpi, with five of the seven mutants phagocytosed more effectively than wildtype. This is consistent with the original premise of the screen, which was designed to identify mutants with reduced capacity to avoid innate phagocyte attack by screening initially for hypovirulence.

Fungal morphology defects of mutants early during infection does not correlate with altered innate immune responses

Since filaments are more difficult to phagocytose that yeast, and five of the seven hypovirulent mutants had been previously identified as having filamentous growth phenotypes on Spider agar, we sought to determine if they also had problems switching to filamentous morphology *in vivo* in the first few hours of infection (31, 42-45). We imaged hindbrain infections with each mutant and analyzed the amount of yeast-shaped vs. elongated cells at 4-6 hours post infection, as cells switching to filamentous growth would have had time to grow longer but would not yet have a hyphal shape (Fig. S3A). Not unexpectedly, four of the five mutants with reduced *in vitro* filamentation (*rim101*Δ/Δ, *brg1*Δ/Δ, *pep8*Δ/Δ and *apm1*Δ/Δ, but

bioRxiv preprint doi: https://doi.org/10.1101/2025.02.14.638315; this version posted February 15, 2025. The copyright holder for this preprint (which was not certified by peer review) is the author/funder, who has granted bioRxiv a license to display the preprint in perpetuity. It is made available under aCC-BY-NC-ND 4.0 International license.

not *cek1*Δ/Δ) had a reduced number of elongated cells *in vivo* at this early timepoint, with dramatic defects in the *rim101*Δ/Δ, *brg1*Δ/Δ and *pep8*Δ/Δ mutants (Fig. S3B; Table 2, n.b. effect size in table indicated only for those comparisons with $p<0.05$). On the other hand, neither *cek1*Δ/Δ nor the two mutants in the Infectivity class of mutants (*nmd5*Δ/Δ and *mad2*Δ/Δ) had a significant reduction in filamentous growth. Early phagocytosis is associated with inhibition of germination and lower virulence (29, 30), which could be a factor in reduced filamentous growth. However, since *rim101*Δ/Δ was the only one of the four mutants with reduced filamentous growth that was phagocytosed at a higher rate, this suggests that the other three mutants form fewer filaments *in vivo* because they have an intrinsically reduced ability to switch to filamentous growth during infection. Interestingly, there was no concordance between significantly altered innate immune responses (in recruitment or phagocytosis efficiency) and a reduced ability to switch to filamentous growth in the early hours of infection. For instance, *mad2*Δ/Δ and *rim101*Δ/Δ have very similar phagocyte response profiles (Table 1, Group I), but only *rim101*Δ/Δ has a strong and significant morphogenesis defect at this early time point *in vivo* (Table 2).

Table 2: Fungal morphology at 4-6 hpi.

	GROUP I			GROUP II		GROUP III	GROUP IV
Mutant	***rim101* Δ/Δ**	***brg1* Δ/Δ**	***mad2* Δ/Δ**	***pep8* Δ/Δ**	***apm1* Δ/Δ**	***nmd5* Δ/Δ**	***cek1* Δ/Δ**
Morphogenesis *in vivo*	**Down**	**Down**	NO CHANGE	**Down**	**Down**	NO CHANGE	NO CHANGE

Regular text: 0.2<p<0.05	Shaded lightly: Moderate Effect	Green: Decreased relative to WT
Bold: p<0.05	Shaded heavily: Strong Effect	Red: Increased relative to WT

Altered cytokine responses to hypovirulent *Candida* mutants

We reasoned that these altered immune responses might be accompanied by altered expression of proinflammatory cytokines and chemokines. Because immune recruitment and

bioRxiv preprint doi: https://doi.org/10.1101/2025.02.14.638315; this version posted February 15, 2025. The copyright holder for this preprint (which was not certified by peer review) is the author/funder, who has granted bioRxiv a license to display the preprint in perpetuity. It is made available under aCC-BY-NC-ND 4.0 International license.

phagocytosis were altered most profoundly for the *brg1*Δ/Δ, *pep8*Δ/Δ and *nmd5*Δ/Δ mutants, and they belong to different classes of mutants (Table 1), we chose to measure inflammatory gene induction in these infections. We measured expression of two key proinflammatory cytokines (interleukin-1 beta and tumor necrosis factor alpha) and the zebrafish IL-8 homolog, each of which is associated with response to *Candida* infection (46). At 4 hours post infection, there was not a significant induction of pro-inflammatory gene expression (Fig. S4), but there was robust induction of these genes by 24 hpi (Fig. 6). At 24 hpi, fish infected with *brg1*Δ/Δ or *pep8*Δ/Δ showed a significant reduction in *cxcl8b*, *tnfa*, and *il1b* induction, while fish infected with *nmd5*Δ/Δ showed a significant reduction in *cxcl8b* and *il1b* induction, but not *tnfa* (Fig. 6A-C). Fish infected with *nmd5*Δ/Δ+*NMD5* showed a trend for increased proinflammatory chemokine/cytokine production, even compared to SN250, which reached significance for *il1b*. This matches well with the decreased survival of fish infected with this complemented strain and the complete complementation phenotype (Fig. 3C). On the other hand, *cxcl8b*, *tnfa*, and *il1b* expression for *brg1*Δ/Δ+*BRG1* and *pep8*Δ/Δ+*PEP8* tended to be between SN250 and the mutant strain, which matches the partial complementation of virulence exhibited by these strains (Fig. 3 A & B). These decreased proinflammatory gene expression signatures are consistent with the effective phagocytosis of the mutants and their overall reduced virulence.

NMD5 is only required for virulence in the presence of fully-active immune attack

Given that *nmd5*Δ/Δ infections are associated with greater phagocytosis and thus infection containment, and its role in *C. albicans* has not been previously described, we sought to determine if its primary role in virulence is in immune evasion. In *S. cerevisiae, Sc*Nmd5p is required for transport of *Sc*Hog1p and *Sc*Crz1p into the nucleus and *ScNMD5* mutants are

bioRxiv preprint doi: https://doi.org/10.1101/2025.02.14.638315; this version posted February 15, 2025. The copyright holder for this preprint (which was not certified by peer review) is the author/funder, who has granted bioRxiv a license to display the preprint in perpetuity. It is made available under aCC-BY-NC-ND 4.0 International license.

sensitive to salt stress imposed by NaCl, LiCl, $MnCl_2$, and $CaCl_2$ (47-49). We therefore tested if *C. albicans nmd5*Δ/Δ was also sensitive to salt stress, oxidative stress or pH. While *nmd5*Δ/Δ formed smaller colonies on regular YPD plates, its relative ability to grow on YPD was unchanged with any of these stresses (Fig. S5).

We reasoned that if the virulence defect that we observed for *nmd5*Δ/Δ was due to a failure to evade phagocytosis, then limiting the immune response should enhance virulence of this mutant. We tested this in several ways. First, we treated infected fish with dexamethasone, a general immunosuppressant that regulates macrophage activity in zebrafish (50). As expected based on previous results, *nmd5*Δ/Δ was less virulent than SN250 in the control DMSO/vehicle treatment condition (Fig. 7A, p=0.014). Dexamethasone immunosuppression increased the virulence of *nmd5*Δ/Δ and eliminated the difference in virulence between *nmd5*Δ/Δ and its wildtype SN250 control (Fig. 7A, $p_{adj}<0.0006$). We then selectively inactivated NADPH oxidase, knocking down $p47^{phox}$, to reduce phagocyte recruitment to and phagocytosis of *C. albicans* (30). As expected based on previous results, *nmd5*Δ/Δ was less virulent than SN250 in the control STD morpholino condition and SN250 was more virulent in the $p47^{phox}$ morphant fish as compared to the STD control morphants (Fig. 7B; p=0.0002 and p=0.039, respectively). This gene-directed inactivation caused *nmd5*Δ/Δ to become more virulent ($p_{adj}=0.0012$), and eliminated any difference in survival between SN250- and *nmd5*Δ/Δ-infected fish (Fig. 7B). Lastly, we performed yolk infections, as there is a weaker immune response to yolk infection relative to hindbrain infection (51). In yolk infections, we also observed no significant difference in the virulence of *nmd5*Δ/Δ compared to SN250 (Fig. 7C). These three models of reduced immune response/immunosuppresssion consistently show that *nmd5*Δ/Δ is just as virulent as

bioRxiv preprint doi: https://doi.org/10.1101/2025.02.14.638315; this version posted February 15, 2025. The copyright holder for this preprint (which was not certified by peer review) is the author/funder, who has granted bioRxiv a license to display the preprint in perpetuity. It is made available under aCC-BY-NC-ND 4.0 International license.

wildtype SN250 when innate immunity is limited, suggesting that its lack of virulence is due to its failure to evade the immune response.

bioRxiv preprint doi: https://doi.org/10.1101/2025.02.14.638315; this version posted February 15, 2025. The copyright holder for this preprint (which was not certified by peer review) is the author/funder, who has granted bioRxiv a license to display the preprint in perpetuity. It is made available under aCC-BY-NC-ND 4.0 International license.

Discussion

Candida albicans has evolved over many generations with vertebrate hosts and has developed the ability to avoid immune clearance through activities such as filamentous growth, masking of cell wall epitopes, production of a toxin and avoidance of antibody opsonization (6-14). However, we still know little about how each of these abilities affects immune evasion during vertebrate infection and we know even less about which fungal genes and pathways regulate immune evasion. The transparency of the larval zebrafish model is a powerful tool that can be utilized to elucidate the different mechanisms of immune evasion in *C. albicans*, especially combined with its cost-effectiveness. Previous work in this infection model has shown that differential immune recruitment and fungal containment through phagocytosis represent important predictors for the fate of individual hosts (29, 30). These favorable aspects of the model led us to complete the first medium-scale screen of 131 *C. albicans* mutants for virulence, with subsequent analysis for early immune-mediated fungal phagocytosis. This screen characterized several new and known virulence genes as having previously unknown roles in limiting innate immune responses at the infection site. We also identified *NMD5* as a new virulence factor that enables immune evasion.

This is the first single-mutant infection screen of more than 100 individual *C. albicans* mutants in any vertebrate infection model, made possible using a zebrafish model. Very few virulence screens of more than 100 *C. albicans* mutants have been conducted, all using pooled/barcode screening methodology (31, 52, 53). While this is a powerful method, secreted signals and virulence factors that affect the overall environment of the infection site will be missed due to the majority prevalence of cells lacking the phenotype. Pooled virulence screens also score competitive index rather than virulence, per se, potentially missing virulence factors.

bioRxiv preprint doi: https://doi.org/10.1101/2025.02.14.638315; this version posted February 15, 2025. The copyright holder for this preprint (which was not certified by peer review) is the author/funder, who has granted bioRxiv a license to display the preprint in perpetuity. It is made available under aCC-BY-NC-ND 4.0 International license.

We chose a zebrafish larval hindbrain infection model to screen individual mutants because it overcomes these drawbacks, reproduces many aspects of murine disseminated infection, and provides a useful infection route for quantifying phagocyte recruitment and response (27, 30, 54). As expected, due to the limitations of pooled screening, several mutants that are hypovirulent in both murine tail vein infection and in our screen were missed in the previous pooled screens (*rim101*Δ/Δ, *brg1*Δ/Δ, *cek1*Δ/Δ).

Of the seven mutants identified here, only four mutants—in *RIM101*, *BRG1*, *MAD2*, *CEK1*—have been tested in single-strain murine tail vein infections; all of them are hypovirulent (Table S4) (44, 55-57). Pooled screens have identified mild defects in competitive index for each of these other three mutants (31, 42). All of the mutants with intermediate virulence defects in our model that have been tested in mouse tail vein infection are also hypovirulent, suggesting that this class represents a mine of new virulence genes, many of which are uncharacterized with only an ORF number (Table S4). However, the converse is not true and some mutants hypovirulent in the mouse were not hypovirulent in our study, suggesting that there may be some murine-specific virulence factors. The high concordance between mouse and zebrafish results reinforces the conservation of infection mechanisms in both hosts; this suggests that the three genes still untested for virulence in mice (*APM1*, *PEP8* and *NMD5*) are most likely of importance in murine (and human) disease.

The zebrafish has the unique advantage of allowing intravital observation of the early innate immune response, which enabled us to group the hypovirulent mutants into four classes. As expected, our screen revealed that increases in phagocytosis efficiency were associated with lower virulence for most of the mutants (Classes I, III and IV). For some mutant infections, phagocyte numbers were unchanged or decreased, while fungal phagocytosis levels of the

bioRxiv preprint doi: https://doi.org/10.1101/2025.02.14.638315; this version posted February 15, 2025. The copyright holder for this preprint (which was not certified by peer review) is the author/funder, who has granted bioRxiv a license to display the preprint in perpetuity. It is made available under aCC-BY-NC-ND 4.0 International license.

mutants matched or exceeded those of wildtype cells (Classes I, II and III). In these infections, a more robust rapid phagocytosis response may limit later phagocyte recruitment at 4-6 hpi and ultimately result in lower inflammatory gene expression at later timepoints. Consistent with this idea, highly effective phagocytosis correlates with reduced epithelial NF-kB activation during mucosal *Candida* infection, which is also in line with the lower cytokine production found here at 24 hpi (58).

The cell wall and fungal morphology regulate phagocytosis by macrophages and neutrophils, with β-glucan masking and filamentous shape leading to impaired phagocytosis (9, 42). *BRG1* and *PEP8*, both in the Morphogenesis class, have not previously been identified as regulating immune responses, although both are linked to *Candida* virulence. The mechanisms underlying the roles of these genes in regulating early immune responses are unknown, although their putative functions in vesicle transport and biofilm formation both have connections to filamentous growth and surface adhesion proteins that may limit phagocytosis (40, 42, 44, 47, 59). Both mutants produced fewer elongated cells *in vivo*. Since larger filamentous cells are engulfed less efficiently, these minor deficiencies in elongation could lead to earlier fungal phagocytosis (42). These and other mutants may also have alterations in their cell walls that eliminate structural mechanisms for phagocytic evasion, although the only strains with known cell wall defects are *cek1*Δ/Δ, which has more β-glucan exposure and recruits more phagocytes to the infection site, and *rim101*Δ/Δ, which regulates cell wall genes (9, 60, 61). This conservation of phenotypes again suggests that the zebrafish is a good model for examining the effect of altered cell wall on early phagocytosis and immune recruitment—even if zebrafish do not have a direct sequence homolog of the key pattern recognition receptor for exposed β-glucan, Dectin-1 (62).

bioRxiv preprint doi: https://doi.org/10.1101/2025.02.14.638315; this version posted February 15, 2025. The copyright holder for this preprint (which was not certified by peer review) is the author/funder, who has granted bioRxiv a license to display the preprint in perpetuity. It is made available under aCC-BY-NC-ND 4.0 International license.

The most pronounced increase in early phagocytic efficiency occurred in infections of fungi lacking *NMD5*, a mutant in the Infectivity class which is predicted to regulate nuclear protein import and ionic stresses, based on work in baker's yeast (47, 48). The *C. albicans nmd5*Δ/Δ mutant has defects in white-opaque switching and its expression is altered in phagocyte interaction, biofilm growth and osmotic stress (63-69). Its differential expression upon neutrophil and macrophage challenges is consistent with its role in limiting phagocytosis (65, 66, 68, 69). In contrast to its function in baker's yeast, the *C. albicans nmd5*Δ/Δ mutant is not hypersensitive to stress conditions, suggesting a significant divergence in gene function between the species—as has been observed previously (70, 71). Instead, the function of *CaNMD5* is clearly related to immune evasion—the mutant loses its virulence disadvantage when the innate immune response is compromised by any of three methods. Given the likely role of Nmd5p in nuclear import of transcription factors, it will be interesting to identify differential transcription patterns in this mutant that may account for the loss in immune evasion.

Overall, our findings reinforce the relevance of studying *Candida*-innate immune events in zebrafish by intravital imaging, identify several new hypovirulent mutants, describe early immune evasion-related phenotypes for all of the mutants, and characterize *NMD5* as a new and important virulence factor required to limit innate immune phagocytosis. These results highlight the importance of an effective early innate immune response that engulfs *C. albicans* cells rapidly to limit germination during infection. We expect that future intravital timelapse experiments in the zebrafish at high spatio-temporal resolution will further characterize how phagocytes interact with these mutants and thereby shed light on conserved mechanisms that regulate early events in candidiasis in vertebrate hosts.

bioRxiv preprint doi: https://doi.org/10.1101/2025.02.14.638315; this version posted February 15, 2025. The copyright holder for this preprint (which was not certified by peer review) is the author/funder, who has granted bioRxiv a license to display the preprint in perpetuity. It is made available under aCC-BY-NC-ND 4.0 International license.

Methods

C. albicans strains and growth conditions

C. albicans mutant strains for screening were obtained from the Noble library (31) . For infection, strains were grown on yeast-peptone-dextrose (YPD) agar at 30ºC (20 g/L glucose, 20 g/L peptone, 10 g/L yeast extract, 20 g/L agar, Difco, Livonia, MI). Single colonies were picked from plates and inoculated into 5mL liquid YPD and grown overnight on a wheel at 30°C. Overnight cultures were resuspended in PBS (phosphate buffered saline, 5 mM sodium chloride, 0.174 mM potassium chloride, 0.33 mM calcium chloride, 0.332 mM magnesium sulfate, 2 mM HEPES in Nanopure water, pH = 7) and stained with Calcofluor white (750 µg/ml) when necessary. Cultures were washed twice with PBS and the concentration was adjusted to $1x10^7$ CFU/ml in PBS for injection. For imaging, strains were transformed with pENO1-iRFP-NAT^r according to (41). Strains were screened by fluorescence microscopy and flow-cytometry to pick the brightest isolates, and the integration site at the *ENO1* locus was confirmed by PCR as described (41). Full deletion of *RBT1* from SN250 was achieved using the SAT-flipper method as described previously (72) using LiAC transformation. The deletion cassette was generated by integrating 514 bp up and 485 bp downstream of *RBT1* into a pSFS2 derivative (72) and was excised by restriction digest with KpnI and SacI.

Complementation of mutant strains

Complementation constructs were ordered from Genscript (Piscataway, NJ) in the pUC57 backbone and contain the ORF with 200 bp upstream and 50 bp downstream, followed by *C. dubliniensis ARG4* (Fig. S6A). Restriction sites were eliminated from the ORF during gene synthesis. A restriction site was designed within the 200 bp upstream region, an NdeI cutsite at the start of the ORF, a BamHI restriction site in *ARG4* upstream region, and a BglII site in the

bioRxiv preprint doi: https://doi.org/10.1101/2025.02.14.638315; this version posted February 15, 2025. The copyright holder for this preprint (which was not certified by peer review) is the author/funder, who has granted bioRxiv a license to display the preprint in perpetuity. It is made available under aCC-BY-NC-ND 4.0 International license.

downstream *ARG4* region. An *NMD5* complementation construct was ordered from Twist Bioscience (South San Francisco, CA) without *ARG4.* This construct included an upstream XbaI restriction site, a 200 bp *NMD5* upstream region containing an XhoI restriction site, the *NMD5* ORF, the mNeon ORF (73) flanked by NcoI restriction sites and a PacI restriction site, then 50 bp of the *NMD5* downstream region, and a BamHI site in an *ARG4* upstream region. This region was then cloned into the Genscript pUC57 backbone by cutting with the with XbaI and BamHI to remove the *PEP8* region and replace it with the *NMD5* region to get an *NMD5* construct containing *ARG4* (Fig. S6B). For complementation, constructs were cut with the appropriate restriction enzymes, and a LiAC transformation was performed using rescue of the *ARG4* autotrophy as a selection marker. PCR was performed to ensure correct integration. *NMD5* complementation colonies were screened by flow cytometry for mNeon-positive cells. Sequences of the complementation constructs are provided in Table S5. To check for functional complementation of mutants that have known morphogenesis defect (Fig. S1) we assessed growth on Spider media (for *BRG1*, *CEK1*, and *PEP8* strains) or in M199 at pH 4 and pH 8 (for *RIM101* strains). Briefly, to test growth on Spider media, we grew SN250, mutant, and complemented strains overnight at 30°C in 5ml YPD. Overnight cultures were diluted in PBS and 100 µl of $1x10^2$ cells/ml was spread onto Spider plates. Plates were incubated at 30°C and imaged after 7 and 14 days of growth. For *RIM101* strains SN250, *rim101*Δ/Δ, and complemented strains were grown overnight at 30°C in 5 ml YPD. 50 µl of overnight culture was inoculated into M199 pH 4 and pH 8 and grown at 37°C for 4 hours. Strains were then imaged on a Zeiss Axio Observer Z1 microscope (Carl Zeiss Microimaging, Thornwood, NJ) to assess filamentous growth.

Growth of *nmd5*Δ/Δ on different media to assess salt tolerance

bioRxiv preprint doi: https://doi.org/10.1101/2025.02.14.638315; this version posted February 15, 2025. The copyright holder for this preprint (which was not certified by peer review) is the author/funder, who has granted bioRxiv a license to display the preprint in perpetuity. It is made available under aCC-BY-NC-ND 4.0 International license.

Overnight cultures were grown at 30°C in 5 ml YPD. $3x10^7$ cells from the overnight culture was inoculated into 5 ml fresh YPD and incubated on roller drum for 4 hours. After 4 hours, 10-fold serial dilutions were performed out to 10^{-5} in PBS, and 3 µl of the 10^0 to 10^{-5} dilutions was spotted onto plates. Plates include YPD, M199 pH 8, M199 pH 4, YPD + 400 mM NaCl, YPD + 1.5 mM H_2O_2, YPD + 400 mM $CaCl_2$, YPD + 150 mM LiCl, and YPD + 6 mM $MnCl_2$. Plates were incubated at 30°C for 48 hours and imaged after 24- and 48-hours incubation. Strains were spotted in duplicate on two plates and 3 replicates performed.

Table 3 ***Candida albicans*** **strains**

Strain	Parental Strain	Genotype	Reference
*yfg*Δ/Δ (Your Favorite Gene) See Table S1 for complete list of mutant strains	SN152	*ura3Δ-iro1Δ::imm*^{434}*/URA3-IRO1, his1Δ/his1Δ, arg4Δ/arg4Δ., leu2Δ/leu2Δ, yfg*Δ*::C.mLEU2/ yfg*Δ*::C.dHIS1 YFG::C.d.ARG4*	(31)
SN250-iRFP	SN152	*ura3Δ-iro1Δ::imm*^{434}*/URA3-IRO1, his1Δ/his1Δ, arg4Δ/arg4Δ., leu2Δ::C.m.LEU2/leu2Δ::C.d.HIS1, , pENO1-iRFP-NATR*	(31), This Study
*rbt1*Δ/Δ$^{968\text{-}2166}$- iRFP	SN152	*ura3Δ-iro1Δ::imm*^{434}*/URA3-IRO1, his1Δ/his1Δ, arg4Δ/arg4Δ., leu2Δ/leu2Δ , rbt1*Δ$^{967\text{-}2166}$*::C.mLEU2/rbt1*Δ$^{967\text{-}3166}$*::C.dHIS1, pENO1-iRFP-NATR*	(31), This Study
*cht2*Δ/Δ- iRFP	SN152	*ura3Δ-iro1Δ::imm*^{434}*/URA3-IRO1, his1Δ/his1Δ, arg4Δ/arg4Δ., leu2Δ/leu2Δ , cht2::C.mLEU2/cht2::C.dHIS1, pENO1-iRFP-NATR*	(31), This Study
*rim101*Δ/Δ- iRFP	SN152	*ura3Δ-iro1Δ::imm*^{434}*/URA3-IRO1, his1Δ/his1Δ, arg4Δ/arg4Δ., leu2Δ/leu2Δ , rim101::C.mLEU2/rim101::C.dHIS1, pENO1-iRFP-NATR*	(31), This Study
*brg1*Δ/Δ- iRFP	SN152	*ura3Δ-iro1Δ::imm*^{434}*/URA3-IRO1, his1Δ/his1Δ, arg4Δ/arg4Δ.,*	(31), This Study

bioRxiv preprint doi: https://doi.org/10.1101/2025.02.14.638315; this version posted February 15, 2025. The copyright holder for this preprint (which was not certified by peer review) is the author/funder, who has granted bioRxiv a license to display the preprint in perpetuity. It is made available under aCC-BY-NC-ND 4.0 International license.

		leu2Δ/leu2Δ , brg1::C.mLEU2/brg1::C.dHIS1, pENO1-iRFP-NATR	
*cek1*Δ/Δ- iRFP	SN152	*ura3Δ-iro1Δ::imm^{434}/URA3-IRO1, his1Δ/his1Δ, arg4Δ/arg4Δ., leu2Δ/leu2Δ , cek1::C.mLEU2/cek1::C.dHIS1, pENO1-iRFP-NATR*	(31), This Study
*pep8*Δ/Δ- iRFP	SN152	*ura3Δ-iro1Δ::imm^{434}/URA3-IRO1, his1Δ/his1Δ, arg4Δ/arg4Δ., leu2Δ/leu2Δ , pep8::C.mLEU2/pep8::C.dHIS1, pENO1-iRFP-NATR*	(31), This Study
*nmd5*Δ/Δ- iRFP	SN152	*ura3Δ-iro1Δ::imm^{434}/URA3-IRO1, his1Δ/his1Δ, arg4Δ/arg4Δ., leu2Δ/leu2Δ , nmd5::C.mLEU2/nmd5::C.dHIS1, pENO1-iRFP-NATR*	(31), This Study
*apm1*Δ/Δ- iRFP	SN152	*ura3Δ-iro1Δ::imm^{434}/URA3-IRO1, his1Δ/his1Δ, arg4Δ/arg4Δ., leu2Δ/leu2Δ , apm1::C.mLEU2/apm1::C.dHIS1, pENO1-iRFP-NATR*	(31), This Study
*mad2*Δ/Δ- iRFP	SN152	*ura3Δ-iro1Δ::imm^{434}/URA3-IRO1, his1Δ/his1Δ, arg4Δ/arg4Δ., leu2Δ/leu2Δ , mad2::C.mLEU2/mad2::C.dHIS1, pENO1-iRFP-NATR*	(31), This Study
*ece1*Δ/Δ - dtom	BWP17	*ura3::imm434/ura3::imm434, iro1::imm434/iron1::imm434, his1::hisG/his1::hisG, arg4::hisG/arg4::hisG, ece1::HIS2/ece1::ARG4, RPS1/rps1::URA3, ENO1/eno1::dTom-NATR*	(74)
*ece1*Δ/Δ+*ECE1* - dtom	BWP17	*ura3::imm434/ura3::imm434, iro1::imm434/iron1::imm434, his1::hisG/his1::hisG, arg4::hisG/arg4::hisG, ece1::HIS2/ece1::ARG4, RPS1/rps1::URA3-ECE1, ENO1/eno1::dTom-NATR*	(74)
NRG1^{OEX}-iRFP	THE21	*ade2::hisG::/ade2::hisG ura3::imm434/ura3::imm434::URA2-tetO ENO1/eno1::ENO1 tetR –*	(75, 76)

bioRxiv preprint doi: https://doi.org/10.1101/2025.02.14.638315; this version posted February 15, 2025. The copyright holder for this preprint (which was not certified by peer review) is the author/funder, who has granted bioRxiv a license to display the preprint in perpetuity. It is made available under aCC-BY-NC-ND 4.0 International license.

		ScHAP4AD-3XHA-ADE2 pENO1-iRFP-NATR	
rbt1Δ/Δ$^{968-2166}$ +RBT1	*rbt1Δ/Δ$^{968-2166}$*	*ura3Δ-iro1Δ::imm^{434}/URA3-IRO1, his1Δ/his1Δ, arg4Δ/arg4Δ., leu2Δ/leu2Δ, rbt1Δ$^{967-2166}$::C.mLEU2/rbt1Δ$^{967-2166}$::C.dHIS1 RBT1::C.d.ARG4*	This Study
rim101Δ/Δ+RIM101	*rim101Δ/Δ*	*ura3Δ-iro1Δ::imm^{434}/URA3-IRO1, his1Δ/his1Δ, arg4Δ/arg4Δ., leu2Δ/leu2Δ, rim101Δ::C.mLEU2/ rim101Δ::C.dHIS1 RIM101::C.d.ARG4*	This Study
brg1Δ/Δ+BRG1	*brg1Δ/Δ*	*ura3Δ-iro1Δ::imm^{434}/URA3-IRO1, his1Δ/his1Δ, arg4Δ/arg4Δ., leu2Δ/leu2Δ, brg1Δ::C.mLEU2/ brg11Δ::C.dHIS1 BRG11::C.d.ARG4*	This Study
cek1Δ/Δ+CEK1	*cek1Δ/Δ*	*ura3Δ-iro1Δ::imm^{434}/URA3-IRO1, his1Δ/his1Δ, arg4Δ/arg4Δ., leu2Δ/leu2Δ, cek1Δ::C.mLEU2/ cek1Δ::C.dHIS1 CEK1::C.d.ARG4*	This Study
pep8Δ/Δ+PEP8	*pep8Δ/Δ*	*ura3Δ-iro1Δ::imm^{434}/URA3-IRO1, his1Δ/his1Δ, arg4Δ/arg4Δ., leu2Δ/leu2Δ, pep8Δ::C.mLEU2/ pep8Δ::C.dHIS1 PEP8::C.d.ARG4*	This Study
nmd5Δ/Δ+NMD5-mNeon -iRFP	*nmd5Δ/Δ-iRFP*	*ura3Δ-iro1Δ::imm^{434}/URA3-IRO1, his1Δ/his1Δ, arg4Δ/arg4Δ., leu2Δ/leu2Δ, ndm5Δ::C.mLEU2/ nmd5::C.dHIS1 NMD5-mNeon::C.d.ARG4, pENO1-iRFP-NATR*	This Study
amp1Δ/Δ+APM1	*apm1Δ/Δ*	*ura3Δ-iro1Δ::imm^{434}/URA3-IRO1, his1Δ/his1Δ, arg4Δ/arg4Δ., leu2Δ/leu2Δ, apm21Δ::C.mLEU2/ apm1Δ::C.dHIS1 APM1::C.d.ARG4*	This Study
mad2Δ/Δ+MAD2	*mad2Δ/Δ*	*ura3Δ-iro1Δ::imm^{434}/URA3-IRO1, his1Δ/his1Δ, arg4Δ/arg4Δ., leu2Δ/leu2Δ, mad2Δ::C.mLEU2/ mad2Δ::C.dHIS1 MAD2::C.d.ARG4*	This Study
rbt1Δ/Δ	SN250	*ura3Δ-iro1Δ::imm^{434}/URA3-IRO1, his1Δ/his1Δ, arg4Δ/arg4Δ., leu2Δ::C.m.LEU2/leu2Δ::C.d.HIS1, rbt1Δ$^{1-2166}$/Δ$^{1-2166}$*	This Study

476

477 Zebrafish Care and Maintenance

bioRxiv preprint doi: https://doi.org/10.1101/2025.02.14.638315; this version posted February 15, 2025. The copyright holder for this preprint (which was not certified by peer review) is the author/funder, who has granted bioRxiv a license to display the preprint in perpetuity. It is made available under aCC-BY-NC-ND 4.0 International license.

Adult zebrafish were held in the University of Maine Zebrafish facility at 28°C in a recirculating system (Aquatic Habitats, Apopka Fl) under a 14 hr/10 hr light/dark cycle and fed Hikari micropellets (catalogue number HK40; Pentair Aquatic Ecosystems).

Ethics Statement

All zebrafish studies were carried out in accordance with the recommendations in the Guide for the Care and Use of Laboratory Animals of the National Research Council (77). All animals were treated in a humane manner and euthanized with Tricaine overdose according to guidelines of the University of Maine Institutional Animal Care and Use Committee (IACUC) as detailed in protocols A2015-11-03, A2018-10-01 and A2021-09-01.

Table 4: Zebrafish lines

Zebrafish Line	Allele	Source/Reference
AB (Wild Type)	n/a	Zebrafish International Resource Center
Tg(mpeg1:EGFP)/ Tg(lysC:dsRed)	gl22Tg nz50Tg	(78, 79)

Zebrafish Infections

Zebrafish were raised at 33°C for the first 24 hours, in E3 plus 0.3 mg/L methylene blue for the first 6 hours then E3 plus PTU (0.02 mg/ml, Sigma-Aldrich, St. Louis, Missouri) thereafter. At 24 hpf, embryos were dechorionated. Injection solutions were made up at $1x10^7$ cells/ml in PBS and stained with Calcofluor white (750 µg/mL) as necessary to visualize non-fluorescent or far-red candida by eye. Embryos were anesthetized in tricaine (160 µg/ml; Tricaine; Western Chemicals, Inc., Ferndale, WA) at the prim-25 stage for both hindbrain and yolk infection (54). Embryos that were injured during the injection process were removed. After infection fish were

bioRxiv preprint doi: https://doi.org/10.1101/2025.02.14.638315; this version posted February 15, 2025. The copyright holder for this preprint (which was not certified by peer review) is the author/funder, who has granted bioRxiv a license to display the preprint in perpetuity. It is made available under aCC-BY-NC-ND 4.0 International license.

placed at 30°C for the remainder of the experiment and monitored for survival out to 72 hpi. Fish were screened after injection on a Zeiss Axio Observer Z1 microscope (Carl Zeiss Microimaging, Thornwood, NJ) to ensure that they received between 10-25 *C. albicans* cells. For large scale virulence screening, 5 *C. albicans* mutants were tested along with SN250 WT control and PBS mock infected fish in one experiment with approximately 50 fish per strain. Due to the large number of injected fish, fish were not screened after injection and *C. albicans* was not stained with Calcofluor white. As another check, if survival of SN250 infected fish fell outside of 5.3-72.18% survival (by 72 hpi) the experiment was eliminated from consideration, and all mutant strains were retested.

Dexamethasone treatment

For dexamethasone experiments, dexamethasone (Millipore Sigma, Calbiochem, 10 mg/ml stock) or DMSO (vehicle control) was added to the E3+PTU one hour before infection and maintained throughout the experiment. A final concentration of 50 µg/ml dexamethasone, 0.5% DMSO was used. Injections in the hindbrain ventricle were otherwise performed as described above.

Morpholino injection

Embryos were injected between the 1- and 4- cell stage with standard (1 ng/nl, CCTCTTACCTCAGTTACAATTTATA) or p47^{phox} (2.5 ng/nl, CGGCGAGATGAAGTGTGTGAGCGAG) morpholinos. Morpholino injection solutions were prepared in 0.3x Danieau buffer (17.4 mM NaCl, 0.21 mM KCl, 0.12 mM $MgSO_4 \cdot 7H_2O$, 0.18 mM $Ca(NO_3)_2$, 1.5 mM Hepes pH 7.2) with 0.16% fluorescent dextran and 0.001% phenol red. Morpholino injected fish were kept in plain E3 until 12 hpf, when methylene blue and PTU

bioRxiv preprint doi: https://doi.org/10.1101/2025.02.14.638315; this version posted February 15, 2025. The copyright holder for this preprint (which was not certified by peer review) is the author/funder, who has granted bioRxiv a license to display the preprint in perpetuity. It is made available under aCC-BY-NC-ND 4.0 International license.

(0.02 mg/ml) was added. At time of infection, fish were switched to E3+PTU and maintained in E3+PTU throughout infection. Fish were screened for dextran incorporation and discarded from the experiment if they did not show fluorescence throughout the fish. Hindbrain infections in morphant fish were performed at the prim-25 stage as described above.

Quantitative real-time PCR

Fish were infected as described above, screened for correct inoculum (10-25 fungal cells), and euthanized at 4 hpi or 24 hpi for qPCR. Pools of 5-10 larvae were homogenized in TRIzol (Invitrogen, Carlsbad, CA) and stored at -80ºC. RNA isolation was performed using the Direct-zol RNA MinipPrep kit (Zymo Research, Irvine, CA) following their protocol. cDNA was synthesized from 500 ng of RNA using iSCRIPT reverse transcription (RT) supermix for RT-qPCR (Bio-Rad, Hercules, CA). qPCR was performed using SsoAdvanced Universal SYBR Green Supermix (Bio-Rad) with 1 µl of cDNA in 10 µl reactions with primers listed in the table below. qPCR was run on a CFX96 Real time system, C1000 touch thermal cycler (Bio-Rad).

Table 5: qPCR primers

Gene	Sequence	Reference
cxcl8b	Fw: GCTGGATCACACTGCAGAAA Rv: TGCTGCAAA CTTTTCCTTGA	(80)
tnfa	Fw: TTCACGCTCCATAAGACCCA Rv: CCGTAGGATTCAGAAAAGCG	(81)
il1b	Fw: GTCACACTGAGAGCCGGAAG Rv: TGGAGATTCCCAAACACACA	(58)
gapdh	Fw: TGGGCCCATGAAAGGAAT Rv: ACCAGCGTCAAAGATGGATG	(82)

Fluorescence Microscopy

bioRxiv preprint doi: https://doi.org/10.1101/2025.02.14.638315; this version posted February 15, 2025. The copyright holder for this preprint (which was not certified by peer review) is the author/funder, who has granted bioRxiv a license to display the preprint in perpetuity. It is made available under aCC-BY-NC-ND 4.0 International license.

For analysis of the phagocyte response at 4-6 hpi, embryos were placed in 0.4% low melting point agarose in E3 with 160 µg/ml tricaine in a glass bottom 24-well plate (MatTek Corporation, Ashland, MA) and the hindbrain ventricle imaged. Images were taken on an Olympus IX-81 inverted microscope with an FV-1000 laser scanning confocal system (Olympus, Waltham, MA) with a 20x (0.75 NA) objective with 5 µm increments for approximately 25-35 slices.

Image Analysis

Images were imported into Fiji (ImageJ) and made into composite 4-channel z-stacks for quantification. Number of *mpeg1*:GFP+ or *lysC*:dsRed+ cells were counted manually for the hindbrain region throughout the z-stack. In addition, *C. albicans* cells were manually counted for whether they were intracellular (inside *mpeg1*:GFP+, *lysC*:dsRed+, or other), or extracellular to determine the percent of *C. albicans* cells that were taken up by the host. The total number of cells recruited to the infection included *mpeg1*:GFP+ cells, *lysC*:dsRed+ cells, as well as non-fluorescent cells phagocytosing *Candida*. Fish were excluded from the total cells recruited count if they did not contain both GFP+ and dsRed+ cells.

Statistical Analysis

Statistical analysis was performed using GraphPad Prism software. To calculate the z-score for quantifying screening results, we measured the mean and standard deviation of 72 hpi percent survival for all of the SN250 (control) infections and then calculated [(Survival % Mutant) – (Mean Survival % Control)] / Standard Deviation of Survival % Control. For analysis of survival in non-screen experiments, Kaplan-Meier curves were generated from at least 3 pooled

bioRxiv preprint doi: https://doi.org/10.1101/2025.02.14.638315; this version posted February 15, 2025. The copyright holder for this preprint (which was not certified by peer review) is the author/funder, who has granted bioRxiv a license to display the preprint in perpetuity. It is made available under aCC-BY-NC-ND 4.0 International license.

563 experiments with the same mutant *C. albicans* strains, with SN250 always included in the same
564 experiments, and Mantel-Cox log rank tests were performed. We utilized Bonferroni corrections
565 to reduce the family-wide error rate in exploratory experiments, while omitting this for any
566 hypotheses that were firmly established *a priori* based on data prior to these experiments (83).
567 Non-exploratory hypotheses based on data shown in Fig. 3 were the following: SN250 is more
568 virulent than *nmd5*Δ/Δ but less virulent than *nmd5*Δ/Δ+*NMD5*, while *nmd5*Δ/Δ is less virulent
569 than both the other strains. Furthermore, we have shown in previous work that p47 morpholino
570 knockdown makes zebrafish more susceptible to wildtype *C. albicans*, so this is confirmatory
571 rather than exploratory (30). Thus, in Fig. 7 the pairwise comparisons shown by arcs (e.g. SN250
572 vs. *nmd5*Δ/Δ) were not Bonferroni corrected for multiple comparisons because the effects of
573 genotype alone were already tested in Fig. 3 and the effect of the p47 MO was already
574 demonstrated (30). For analysis of differences in phagocyte recruitment and phagocytosis, a
575 normality test was performed. If the distribution was not normal, the data was trimmed for
576 outliers (top and bottom 10%) and this allowed for parametric testing. All mutants were
577 compared with wildtype SN250 in each experiment. For simplicity to present all data in one
578 graph, data was normalized to WT, SN250 values. For normalization, the average SN250 value
579 for a set of experiments was divided by the average SN250 value for all experiments, to get an
580 adjustment value. The value for each individual fish was then divided by this adjustment value,
581 to get a normalized value for each fish. Normalized values were used to generate plots, which
582 show the mean and 95% confidence interval. Effect size was determined as described by (84)
583 using the Effect Size Calculator
584 (https://f.hubspotusercontent30.net/hubfs/5191137/attachments/ebe/EffectSizeCalculator.xls). A
585 size of greater than 0 and less than 0.3 was qualified as Small, greater than 0.3 and less than 0.5

bioRxiv preprint doi: https://doi.org/10.1101/2025.02.14.638315; this version posted February 15, 2025. The copyright holder for this preprint (which was not certified by peer review) is the author/funder, who has granted bioRxiv a license to display the preprint in perpetuity. It is made available under aCC-BY-NC-ND 4.0 International license.

as Moderate, and greater than 0.5 as Strong (84). Briefly, this is calculated as $(M_1 - M_2)/ s_{pooled}$, where M_1 -M_2 is the difference between the means and s_{pooled} is the root mean squared of the two standard deviations. Hedges' factor is used to correct for bias in effect size (85).

Acknowledgements

We would like to thank Prof. Suzanne Noble for making the mutant library available through the Fungal Genetics Stock Center, and Mark Nilan for providing wonderful fish care. This work is supported by grants from the University of Maine Institute of Medicine (to BAB), Maine INBRE (Honors Pre-thesis and Thesis Fellowships through NIH P20GM103423 to EB, MM and LS), and R15AI169393 (to RTW). RTW is a Burroughs Welcome Fund Investigator in the Pathogenesis of Infectious Disease.

bioRxiv preprint doi: https://doi.org/10.1101/2025.02.14.638315; this version posted February 15, 2025. The copyright holder for this preprint (which was not certified by peer review) is the author/funder, who has granted bioRxiv a license to display the preprint in perpetuity. It is made available under aCC-BY-NC-ND 4.0 International license.

598 **Figure Legends**

599

600 **Fig. 1. Defining infection parameters**. **A)** Flow chart showing workflow of pilot experiments.
601 Hindbrain infections were performed at the prim-25 stage, and fish were then screened to ensure
602 they received the correct inoculum (10-25 cells). At 4-6 hours post-infection, fish were imaged
603 by confocal microscopy to score fungal phagocytosis; survival was monitored out to 72 hpi. **B)**
604 Example Kaplan-Meier survival curves pooled from 3 experiments showing fish injected with
605 PBS (Control, n=83), SN250 (WT, n=61), *adr1*Δ/Δ (n=63), or *mad2*Δ/Δ (n=57). Fish injected
606 with *mad2*Δ/Δ showed increased survival compared to SN250 (p=0.0001). **C)** Survival of fish
607 injected with each strain at 72 hpi in three independent experiments. Individual points represent
608 biologically independent experiments on different days. Bars show means and standard
609 deviations with SN250 in red to depict WT cutoff range for inclusion of experiments. Significant
610 differences in survival curves were determined by Mantel-Cox log rank tests comparing the
611 mutant strain to SN250 from data pooled from three biological replicates of the same
612 experiments. Two mutants were tested per experiment, and Bonferroni corrections were
613 performed. **D)** Representative images of hindbrain ventricle infection to score fungal
614 phagocytosis at 4 hpi. *C. albicans* initial inoculum was stained with Calcofluor white, shown in
615 blue. The hindbrain ventricle is outlined by a white dashed line. Scalebar is 50 μm. Arrows point
616 to extracellular *Candida*, while arrowheads point to intracellular *Candida*. **E)** Quantification of
617 the percent of intracellular *Candida*. Fungal cells were scored as intracellular or extracellular
618 from z-stack slices (using Calcofluor fluorescence for the fungi and differential interference
619 contrast (DIC) for imaging the phagocytes) of individual fish taken at 4-6 hpi for each strain.
620 Based on at least 19 fish from at least 3 independent experiments. Significance and effect size

bioRxiv preprint doi: https://doi.org/10.1101/2025.02.14.638315; this version posted February 15, 2025. The copyright holder for this preprint (which was not certified by peer review) is the author/funder, who has granted bioRxiv a license to display the preprint in perpetuity. It is made available under aCC-BY-NC-ND 4.0 International license.

were determined as described in Materials & Methods and based on (84). * p<0.05, ** p<0.01, *** p<0.001.

Fig. 2. High-throughput virulence screening. Average survival of fish infected with individual mutant *C. albicans* strains (n ≈ 50 fish per mutant strain). Mock infected (PBS) and NRG1^{OEX} infected fish were included as controls. The average survival of the WT SN250 strain is shown by the black line, while differential survival was measured by Z-score (based on the standard deviation of % survival in over 20 experiments with SN250 control infections). Gray lines show Z-score = 1, blue lines show Z-score = 2, and red Z-score = 3. Strains in the red panel were previously seen to have a morphogenesis defect on spider agar, while those in the blue panel showed a defect in pooled virulence tests, and those in the green panel code for predicted secreted proteins. Mutant strains that had a z-score of over 3 were passed to the next phase of screening, shown as squares. Those where both independent mutants showed hypovirulence genotyped correctly, and complementation restored virulence, are shown as filled in squares and were passed to the imaging phase of screening. Those that did not pass secondary screening are shown as empty squares. Complete data is found in Supplementary Table S1.

Fig. 3. Complementation restores virulence to hypovirulent *C. albicans* mutants. Kaplan-Meier survival curves show restoration of virulence of with complementation. All data in survival curves are pooled from 2 experiments unless otherwise noted. **A)** Fish injected with SN250 (WT, n=37), *brg1*Δ/Δ (n=37), *brg1*Δ/Δ+*BRG1* (n=45), PBS (mock, n= 20). Complementation of *brg1*Δ/Δ restores some virulence. **B)** Fish injected with SN250 (WT, n=49), *pep8*Δ/Δ (n=75), *pep8*Δ/Δ+*PEP8* (n=57), or PBS (mock, n= 30). Complementation of

bioRxiv preprint doi: https://doi.org/10.1101/2025.02.14.638315; this version posted February 15, 2025. The copyright holder for this preprint (which was not certified by peer review) is the author/funder, who has granted bioRxiv a license to display the preprint in perpetuity. It is made available under aCC-BY-NC-ND 4.0 International license.

644 *pep8*Δ/Δ restores some virulence (data pooled from 3 experiments). **C)** Fish injected with PBS
645 (mock, n=20), SN250 (WT, n=37), *nmd5*Δ/Δ (n=44), *nmd5*Δ/Δ+NMD5 (n=41).
646 Complementation significantly increases virulence of *nmd5*Δ/Δ. **D)** Fish injected with SN250
647 (WT, n= 45), *rim101*Δ/Δ (n=43), *rim101*Δ/Δ+*RIM101* (n=41), or mock infected fish (PBS,
648 n=20). Complementation of *rim101*Δ/Δ restores virulence (Data pooled from 3 independent
649 experiments). **E)** Fish injected with SN250 (WT, n=35), *cek1*Δ/Δ (n=41), *cek1*Δ/Δ+*CEK1*
650 (n=45), or mock infected fish (PBS, n= 19). Complementation of *cek1*Δ/Δ restores virulence. **F)**
651 Fish injected with PBS (mock, n=21), SN250 (WT, n=34), *apm1*Δ/Δ (n=39), or *apm1*Δ/Δ+*APM1*
652 (n=28). Complementation significantly increases virulence of *apm1*Δ/Δ. **G)** Fish injected with
653 PBS (mock, n=18), SN250 (WT, n=40), *mad2*Δ/Δ (n=43), or *mad2*Δ/Δ+*MAD2* (n=39).
654 Complementation significantly increases virulence of *mad2*Δ/Δ. * $p_{adj} < 0.05$, **, $p_{adj} < 0.01$,
655 ***, $p_{adj} < 0.001$
656
657 **Fig. 4. Phagocyte recruitment to hypovirulent *C. albicans* mutants. A)** Example
658 representative images from *brg1*Δ/Δ- *pep8*Δ/Δ and *cek1*Δ/Δ-infected fish, along with SN250-
659 infected controls, at 4-6 hours post-infection. Images were scored by eye for the number of
660 macrophages (*mpeg1*:GFP+ cells) shown in green and number of neutrophils (*lysC*:dsRed+ cells)
661 in magenta recruited to the infection, as well as if the *Candida* was intracellular or extracellular.
662 Scalebar is 100 μm. **B-D)** Quantification of phagocyte recruitment-related phenotypes. There are
663 separate SN250 columns for each set of experiments, as the mutant was compared to wildtype in
664 the same experiments. **B)** Plots showing the number of *mpeg*:GFP+ macrophages recruited to the
665 infection site normalized to the average amount of *mpeg*:GFP+ macrophages recruited to SN250.
666 **C)** Plots showing the number of *lysC*:dsRed+ neutrophils recruited to the infection site

bioRxiv preprint doi: https://doi.org/10.1101/2025.02.14.638315; this version posted February 15, 2025. The copyright holder for this preprint (which was not certified by peer review) is the author/funder, who has granted bioRxiv a license to display the preprint in perpetuity. It is made available under aCC-BY-NC-ND 4.0 International license.

667 normalized to the average amount of *lysC*:dsRed+ neutrophils recruited to SN250. **D)** Plots
668 showing the number of cells recruited to the infection site normalized to the average recruited to
669 SN250. Cells include *mpeg1*:GFP+ and *lysC*:dsRed+ cells recruited to the hindbrain, as well as
670 non-fluorescent cells containing *Candida*. **(B-D)** Shading indicates the Groups I-IV, based on
671 similar interaction phenotypes (Table 1). Means and 95% confidence intervals are plotted.
672 Statistics were performed from data pooled from at least 3 independent experiments for each
673 mutant, for approximately 25 fish per strain were imaged. Hedges bias-corrected effect sizes and
674 significance was determined for each mutant. * indicates $p<0.05$, # indicates a moderate effect,
675 while a bold # indicates a strong effect.
676
677 **Fig. 5. Phagocytosis of hypovirulent *C. albicans* mutants. A)** Example representative images
678 from *nmd5*Δ/Δ- *rim101*Δ/Δ and *mad2*Δ/Δ-infected fish, along with SN250-infected controls, at 4-
679 6 hours post-infection. Images were scored by eye for the number of macrophages (Mpeg1-
680 GFP+ cells) shown in green and number of neutrophils (LysC-dsRed+ cells) in magenta
681 recruited to the infection, as well as if the *Candida* was intracellular or extracellular. Scalebar is
682 100 μm. **B-D)** Quantification of phagocytosis-related phenotypes. There are separate SN250
683 columns for each set of experiments, as the mutant was compared to wildtype in the same
684 experiments. **B)** Plots of the percent intracellular *Candida* normalized to the average percent
685 intracellular *Candida* for SN250. **C)** Plots showing the number extracellular *Candida* normalized
686 to the average amount for SN250. **D)** Plots showing the number of intracellular *Candida*, divided
687 by the number of cells recruited, normalized to the average for SN250. **(B-D)** Shading indicates
688 the Groups I-IV, based on similar interaction phenotypes (Table 1). Means and 95% confidence
689 intervals are plotted. Statistics were performed from pooled data from at least 3 independent

bioRxiv preprint doi: https://doi.org/10.1101/2025.02.14.638315; this version posted February 15, 2025. The copyright holder for this preprint (which was not certified by peer review) is the author/funder, who has granted bioRxiv a license to display the preprint in perpetuity. It is made available under aCC-BY-NC-ND 4.0 International license.

690 experiments for each mutant, for approximately 25 fish per strain imaged. Hedges bias-corrected
691 effect sizes and significance was determined for each mutant. * indicates $p<0.05$, # indicates a
692 moderate effect, while a bold # indicates a strong effect.
693
694 **Fig. 6. Hypovirulent *C. albicans* mutants elicit a reduced proinflammatory expression at 24**
695 **hours post infection.** Expression of *cxcl8b* (**A**), *tnfa* (**B**), or *il1b* (**C**) by qPCR analysis of fish
696 infected with WT (SN250), mutant (*nmd5*Δ/Δ, *brg1*Δ/Δ, or *pep8*Δ/Δ), or complemented
697 (*nmd5*Δ/Δ+NMD5, *brg1*Δ/Δ+BRG1, or *pep8*Δ/Δ+PEP8) *C. albicans* at 24 hpi. Each point
698 represents a pool of at least 5 larvae, and data was pooled from 3 (*NMD5*) or 4 (*BRG1* & *PEP8*)
699 independent experiments. Gene expression was normalized to *gapdh* and induction was
700 determined relative to PBS mock infected larvae. Significance was determined by one-way
701 ANOVA with Dunnett's multiple comparisons tests.
702
703 **Figure 7 *nmd5*Δ/Δ has fully restored virulence in fish with a reduced immune response A)**
704 Kaplan-Meier survival curve of dexamethasone treated hindbrain injected fish with PBS (n=28),
705 SN250 (n=41), *nmd5*Δ/Δ (n=43), or *nmd5*Δ/Δ+*NMD5* (n=35) or DMSO fish injected with PBS
706 (n=28), SN250 (n=36), *nmd5*Δ/Δ (n=43), or *nmd5*Δ/Δ+*NMD5* (n=43). Data pooled from 3
707 independent experiments. **B)** Kaplan-Meier survival curve of standard morphant fish injected
708 with PBS (n=22), SN250 (n=46), *nmd5*Δ/Δ (n=39), or *nmd5*Δ/Δ+*NMD5* (n=35), and p47
709 morphant fish injected with PBS (n=20), SN250 (n=59), *nmd5*Δ/Δ (n=26), or *nmd5*Δ/Δ+*NMD5*
710 (n=34). Data pooled from 4 independent experiments. **C)** Kaplan-Meier survival curve of PBS
711 (n=34), SN250 (n=37), or *nmd5*Δ/Δ (n=34) yolk injected fish. Data pooled from 2 independent
712 experiments. Statistics were performed as described in detail in Materials & Methods. Pairwise

bioRxiv preprint doi: https://doi.org/10.1101/2025.02.14.638315; this version posted February 15, 2025. The copyright holder for this preprint (which was not certified by peer review) is the author/funder, who has granted bioRxiv a license to display the preprint in perpetuity. It is made available under aCC-BY-NC-ND 4.0 International license.

comparisons that are shown by arcs are confirmatory based on previous experiments; those shown by brackets are exploratory and adjusted for multiple comparisons by Bonferroni correction. Square brackets show if there is an effect of an immune perturbation on survival; curved brackets show if there is an effect of genotype on survival in the context of an immune perturbation. N.s. $p_{adj} > 0.05$ * $p_{adj} < 0.05$, **, $p_{adj} < 0.01$, ***, $p_{adj} < 0.001$.

Supplementary Figures

Fig. S1. Complementation partially restores *in vitro* phenotypes of *brg1*Δ/Δ, *pep8*Δ/Δ, *cek1*Δ/Δ and *rim101*Δ/Δ mutants. Growth of SN250 (**A-C**), *brg1*Δ/Δ, *brg1*Δ/Δ+*BRG1* (**A**), *pep8*Δ/Δ, *pep8*Δ/Δ+*PEP8* (**B**), *cek1*Δ/Δ, and *cek1*Δ/Δ+*CEK1* (**C**) on Spider agar after 7 and 14 days at 30°C. **D)** Growth of SN250, *rim101*Δ/Δ, and *rim101*Δ/Δ+*RIM101* in M199 pH 4 or pH 8 after 4 hours at 37°C. Scale bar is 20 μm.

Fig. S2. Complementation did not restore virulence of *cht2*Δ/Δ, *orf19.5547*Δ/Δ, or *rbt1*$^{968\text{-}2166}$Δ/Δ. A) Kaplan-Meier survival curve of fish injected with PBS (mock, n=23), SN250 (WT, n=41), *cht2*Δ/Δ (n=31), or *cht2*Δ/Δ+*CHT2* (n=44). Data pooled from 2 experiments. **B)** Kaplan-Meier survival curve of fish injected with PBS (mock, n=10), SN250 (WT, n=21), *orf19.5547*Δ/Δ (n=16), or *orf19.5547*Δ/Δ+*ORF19.5547* (n=19). Data from 1 experiment. **C)** Kaplan-Meier survival curve of fish injected with PBS (mock, n=58), SN250 (WT, n=84), *rbt1*$^{968\text{-}2166}$Δ/Δ (n=90), or *rbt1*$^{968\text{-}2166}$Δ/Δ+*RBT1* (n=105). Data pooled from 5 experiments. **D)** Kaplan-Meier survival curve of fish injected with PBS (mock n=35), SN250 (WT, n=60), *rbt1*$^{968\text{-}2166}$Δ/Δ (n=52), or *rbt1*Δ/Δ (n=60). Data pooled from 3 experiments.

bioRxiv preprint doi: https://doi.org/10.1101/2025.02.14.638315; this version posted February 15, 2025. The copyright holder for this preprint (which was not certified by peer review) is the author/funder, who has granted bioRxiv a license to display the preprint in perpetuity. It is made available under aCC-BY-NC-ND 4.0 International license.

Fig. S3. ***brg1*Δ/Δ and *pep8*Δ/Δ show fewer elongated cells in the zebrafish hindbrain at 4-6 hours post infection. A)** Images of SN250 and *brg1*Δ/Δ infected fish showing yeast (arrow heads) and elongated cells (arrows) in the zebrafish hindbrain at 4-6 hours post infection. Scalebars are 50 μm. **B)** Plot showing the percent of elongated cells for each mutant with the control SN250 for the same experiments. The number of yeast and elongated cells was counted manually in at least 3 independent experiments for each mutant, with approximately 25 fish per strain imaged. There are separate SN250 columns for each set of experiments, as the mutant was compared to wildtype in the same experiments. Shading indicates the Groups I-IV, based on similar fungal-immune interaction phenotypes (Table 1). Means and 95% confidence intervals are plotted. Hedges bias-corrected effect sizes and significance was determined for each mutant. * indicates $p<0.05$, *** indicates $p<0.001$, # indicates a moderate effect, ## indicates a large effect.

Fig. S4. Expression of inflammatory genes early during *C. albicans* infection. Zebrafish larvae at the prim25 stage were infected with 10-25 *C. albicans* cells of the wildtype SN250 strain. At 4-6 hours post-infection, they were euthanized, RNA was purified, and qPCR was conducted to determine the change in gene expression relative to the mock-infected controls at the same time point. There was no significant induction of any of these inflammatory genes at this timepoint, although there was a slight reduction in *ccl2* expression. Shown are averages and 95% confidence intervals for seven biologically independent experiments. Significant changes were determined by comparing the 95% confidence intervals; none were significantly up-regulated.

bioRxiv preprint doi: https://doi.org/10.1101/2025.02.14.638315; this version posted February 15, 2025. The copyright holder for this preprint (which was not certified by peer review) is the author/funder, who has granted bioRxiv a license to display the preprint in perpetuity. It is made available under aCC-BY-NC-ND 4.0 International license.

Figure S5 *nmd5*Δ/Δ is not more susceptible to cell stressors. Growth of SN250, *nmd5*Δ/Δ, and *nmd5*Δ/Δ+*NMD5* on YPD, M199 pH 8, M199 pH 4, YPD + 400 mM NaCl, YPD + 1.5 mM H_2O_2, YPD + 400 mM $CaCl_2$, YPD + 150 mM LiCl, and 6 mM $MnCl_2$. $3x10^7$ cells from the overnight culture was inoculated into 5ml fresh YPD and incubated on roller drum for 4 hours. After 4 hours 10-fold serial dilutions 3µl of the dilutions was spotted onto plates. Plates were incubated at 30°C for 48 hours and imaged after 24- and 48-hours incubation.

Fig. S6. Complementation Constructs A) Plasmid showing the design of the construct for complementation of mutant strains. All plasmids contained a BglII cut site downstream of *ARG4*, a BamHI cutsite upstream of *ARG4*, an NdeI cutsite at the ORF start site, and another restriction cut site in the complementary upstream region of the gene of interest. The upstream restriction site and the BglII restriction site were used to excise the fragment for complementation. **B)** Plasmid showing the design of the construct for complementation of *nmd5*Δ/Δ. The *NMD5* complementation construct contains mNeon to enable screening of transformants for fluorescence to assess functional complementation. The XhoI and BglII restriction sites were used to excise the fragment for complementation. Sequences of ORFs with upstream and downstream regions used in complementation constructs is provided in Table S5.

Table S1. Full list of *C. albicans* strains used in this study. All mutants tested in this study and which stages of testing they passed.

bioRxiv preprint doi: https://doi.org/10.1101/2025.02.14.638315; this version posted February 15, 2025. The copyright holder for this preprint (which was not certified by peer review) is the author/funder, who has granted bioRxiv a license to display the preprint in perpetuity. It is made available under aCC-BY-NC-ND 4.0 International license.

Table S2. Phagocytosis efficiency for Calcofluor White-labeled mutant *C. albicans* infections. Summary statistics of the immune response to infection for all mutant *C. albicans* infections imaged, as shown in Fig. 1E.

Table S3. Immune response to mutant *C. albicans* infections. Summary statistics of the immune response to infection for all mutant *C. albicans* infections imaged in double transgenic fish, as shown in Fig. 4 and Fig. 5.

Table S4. Comparison of mutant virulence in zebrafish hindbrain infection versus mouse tail vein infection. Breakdown of virulence phenotypes for all mutants included in this screen.

Table S5. Complementation Construct Sequences. Sequences used for complementation for each mutant, as well as *C. dubliniensis ARG4* used in each of the complementation constructs. Complementation constructs were constructed by inserting these sequences into the pUC57 vector.

bioRxiv preprint doi: https://doi.org/10.1101/2025.02.14.638315; this version posted February 15, 2025. The copyright holder for this preprint (which was not certified by peer review) is the author/funder, who has granted bioRxiv a license to display the preprint in perpetuity. It is made available under aCC-BY-NC-ND 4.0 International license.

References

1. Benedict K, Jackson BR, Chiller T, Beer KD. 2019. Estimation of Direct Healthcare Costs of Fungal Diseases in the United States. Clin Infect Dis 68:1791-1797.

2. Tsay S, Williams S, Mu Y, Epson E, Johnston H, Farley MM, Harrison LH, Vonbank B, Shrum S, Dumyati G, Zhang A, Schaffner W, Magill S, Vallabhaneni S. 2018. National Burden of Candidemia, United States, 2017. Open Forum Infectious Diseases 5:S142-S143.

3. Ardizzoni A, Wheeler RT, Pericolini E. 2021. It Takes Two to Tango: How a Dysregulation of the Innate Immunity, Coupled With Candida Virulence, Triggers VVC Onset. Front Microbiol 12:692491.

4. Brown GD, Denning DW, Gow NA, Levitz SM, Netea MG, White TC. 2012. Hidden killers: human fungal infections. Sci Transl Med 4:165rv13.

5. Smith DJ, Gold JAW, Benedict K, Wu K, Lyman M, Jordan A, Medina N, Lockhart SR, Sexton DJ, Chow NA, Jackson BR, Litvintseva AP, Toda M, Chiller T. 2023. Public Health Research Priorities for Fungal Diseases: A Multidisciplinary Approach to Save Lives. J Fungi (Basel) 9.

6. Brown R, Priest E, Naglik JR, Richardson JP. 2021. Fungal Toxins and Host Immune Responses. Front Microbiol 12:643639.

7. Goyal S, Castrillon-Betancur JC, Klaile E, Slevogt H. 2018. The Interaction of Human Pathogenic Fungi With C-Type Lectin Receptors. Front Immunol 9:1261.

8. Hernandez-Chavez MJ, Perez-Garcia LA, Nino-Vega GA, Mora-Montes HM. 2017. Fungal Strategies to Evade the Host Immune Recognition. J Fungi (Basel) 3.

bioRxiv preprint doi: https://doi.org/10.1101/2025.02.14.638315; this version posted February 15, 2025. The copyright holder for this preprint (which was not certified by peer review) is the author/funder, who has granted bioRxiv a license to display the preprint in perpetuity. It is made available under aCC-BY-NC-ND 4.0 International license.

9. Hopke A, Brown AJP, Hall RA, Wheeler RT. 2018. Dynamic Fungal Cell Wall Architecture in Stress Adaptation and Immune Evasion. Trends Microbiol 26:284-295.

10. Kadosh D. 2019. Regulatory mechanisms controlling morphology and pathogenesis in Candida albicans. Curr Opin Microbiol 52:27-34.

11. Oliver JC, Ferreira C, Silva NC, Dias ALT. 2019. Candida spp. and phagocytosis: multiple evasion mechanisms. Antonie Van Leeuwenhoek 112:1409-1423.

12. Ost KS, O'Meara TR, Stephens WZ, Chiaro T, Zhou H, Penman J, Bell R, Catanzaro JR, Song D, Singh S, Call DH, Hwang-Wong E, Hanson KE, Valentine JF, Christensen KA, O'Connell RM, Cormack B, Ibrahim AS, Palm NW, Noble SM, Round JL. 2021. Adaptive immunity induces mutualism between commensal eukaryotes. Nature 596:114-118.

13. Seider K, Heyken A, Luttich A, Miramon P, Hube B. 2010. Interaction of pathogenic yeasts with phagocytes: survival, persistence and escape. Curr Opin Microbiol 13:392-400.

14. Singh DK, Toth R, Gacser A. 2020. Mechanisms of Pathogenic Candida Species to Evade the Host Complement Attack. Front Cell Infect Microbiol 10:94.

15. Brown GD. 2011. Innate antifungal immunity: the key role of phagocytes. Annu Rev Immunol 29:1-21.

16. Dambuza IM, Levitz SM, Netea MG, Brown GD. 2017. Fungal Recognition and Host Defense Mechanisms. Microbiol Spectr 5.

17. Jawale CV, Biswas PS. 2021. Local antifungal immunity in the kidney in disseminated candidiasis. Curr Opin Microbiol 62:1-7.

18. Lionakis MS, Iliev ID, Hohl TM. 2017. Immunity against fungi. JCI Insight 2.

bioRxiv preprint doi: https://doi.org/10.1101/2025.02.14.638315; this version posted February 15, 2025. The copyright holder for this preprint (which was not certified by peer review) is the author/funder, who has granted bioRxiv a license to display the preprint in perpetuity. It is made available under aCC-BY-NC-ND 4.0 International license.

19. Netea MG, Joosten LA, van der Meer JW, Kullberg BJ, van de Veerdonk FL. 2015. Immune defence against Candida fungal infections. Nat Rev Immunol 15:630-42.

20. Drummond RA, Collar AL, Swamydas M, Rodriguez CA, Lim JK, Mendez LM, Fink DL, Hsu AP, Zhai B, Karauzum H, Mikelis CM, Rose SR, Ferre EM, Yockey L, Lemberg K, Kuehn HS, Rosenzweig SD, Lin X, Chittiboina P, Datta SK, Belhorn TH, Weimer ET, Hernandez ML, Hohl TM, Kuhns DB, Lionakis MS. 2015. CARD9-Dependent Neutrophil Recruitment Protects against Fungal Invasion of the Central Nervous System. PLoS Pathog 11:e1005293.

21. Drummond RA. 2023. What fungal CNS infections can teach us about neuroimmunology and CNS-specific immunity. Semin Immunol 67:101751.

22. Urban CF, Nett JE. 2019. Neutrophil extracellular traps in fungal infection. Semin Cell Dev Biol 89:47-57.

23. da Silva Dantas A, Lee KK, Raziunaite I, Schaefer K, Wagener J, Yadav B, Gow NA. 2016. Cell biology of Candida albicans-host interactions. Curr Opin Microbiol 34:111-118.

24. Jimenez-Lopez C, Lorenz MC. 2013. Fungal immune evasion in a model host-pathogen interaction: Candida albicans versus macrophages. PLoS Pathog 9:e1003741.

25. Williams TJ, Gonzales-Huerta LE, Armstrong-James D. 2021. Fungal-Induced Programmed Cell Death. J Fungi (Basel) 7.

26. Burgess TB, Condliffe AM, Elks PM. 2022. A Fun-Guide to Innate Immune Responses to Fungal Infections. J Fungi (Basel) 8.

bioRxiv preprint doi: https://doi.org/10.1101/2025.02.14.638315; this version posted February 15, 2025. The copyright holder for this preprint (which was not certified by peer review) is the author/funder, who has granted bioRxiv a license to display the preprint in perpetuity. It is made available under aCC-BY-NC-ND 4.0 International license.

27. Rosowski EE, Knox BP, Archambault LS, Huttenlocher A, Keller NP, Wheeler RT, Davis JM. 2018. The Zebrafish as a Model Host for Invasive Fungal Infections. J Fungi (Basel) 4.

28. Tobin DM, May RC, Wheeler RT. 2012. Zebrafish: a see-through host and a fluorescent toolbox to probe host-pathogen interaction. PLoS Pathog 8:e1002349.

29. Bergeron AC, Barker SE, Brothers KM, Prasad BC, Wheeler RT. 2017. Polyclonal anti-Candida antibody improves phagocytosis and overall outcome in zebrafish model of disseminated candidiasis. Dev Comp Immunol 68:69-78.

30. Brothers KM, Gratacap RL, Barker SE, Newman ZR, Norum A, Wheeler RT. 2013. NADPH oxidase-driven phagocyte recruitment controls Candida albicans filamentous growth and prevents mortality. PLoS Pathog 9:e1003634.

31. Noble SM, French S, Kohn LA, Chen V, Johnson AD. 2010. Systematic screens of a Candida albicans homozygous deletion library decouple morphogenetic switching and pathogenicity. Nat Genet 42:590-8.

32. Lewis LE, Bain JM, Lowes C, Gillespie C, Rudkin FM, Gow NA, Erwig LP. 2012. Stage specific assessment of Candida albicans phagocytosis by macrophages identifies cell wall composition and morphogenesis as key determinants. PLoS Pathog 8:e1002578.

33. Mallick EM, Bergeron AC, Jones SK, Jr., Newman ZR, Brothers KM, Creton R, Wheeler RT, Bennett RJ. 2016. Phenotypic Plasticity Regulates Candida albicans Interactions and Virulence in the Vertebrate Host. Front Microbiol 7:780.

34. Braun BR, Head WS, Wang MX, Johnson AD. 2000. Identification and characterization of TUP1-regulated genes in Candida albicans. Genetics 156:31-44.

bioRxiv preprint doi: https://doi.org/10.1101/2025.02.14.638315; this version posted February 15, 2025. The copyright holder for this preprint (which was not certified by peer review) is the author/funder, who has granted bioRxiv a license to display the preprint in perpetuity. It is made available under aCC-BY-NC-ND 4.0 International license.

883 35. Gomez-Gaviria M, Vargas-Macias AP, Garcia-Carnero LC, Martinez-Duncker I, Mora-
884 Montes HM. 2021. Role of Protein Glycosylation in Interactions of Medically Relevant
885 Fungi with the Host. J Fungi (Basel) 7.
886 36. Jia LJ, Gonzalez K, Orasch T, Schmidt F, Brakhage AA. 2024. Manipulation of host
887 phagocytosis by fungal pathogens and therapeutic opportunities. Nat Microbiol 9:2216-
888 2231.
889 37. Uhl MA, Biery M, Craig N, Johnson AD. 2003. Haploinsufficiency-based large-scale
890 forward genetic analysis of filamentous growth in the diploid human fungal pathogen
891 C.albicans. EMBO J 22:2668-78.
892 38. Mao Y, Solis NV, Filler SG, Mitchell AP. 2023. Functional Dichotomy for a Hyphal
893 Repressor in Candida albicans. mBio 14:e0013423.
894 39. Sharma A, Mitchell AP. 2023. Strain variation in gene expression impact of hyphal
895 cyclin Hgc1 in Candida albicans. G3 (Bethesda) 13.
896 40. Solis NV, Wakade RS, Glazier VE, Ollinger TL, Wellington M, Mitchell AP, Filler SG,
897 Krysan DJ. 2022. Systematic Genetic Interaction Analysis Identifies a Transcription
898 Factor Circuit Required for Oropharyngeal Candidiasis. mBio 13:e0344721.
899 41. Bergeron AC, Seman BG, Hammond JH, Archambault LS, Hogan DA, Wheeler RT.
900 2017. Candida albicans and Pseudomonas aeruginosa Interact To Enhance Virulence of
901 Mucosal Infection in Transparent Zebrafish. Infect Immun 85.
902 42. Bain JM, Louw J, Lewis LE, Okai B, Walls CA, Ballou ER, Walker LA, Reid D, Munro
903 CA, Brown AJ, Brown GD, Gow NA, Erwig LP. 2014. Candida albicans hypha
904 formation and mannan masking of beta-glucan inhibit macrophage phagosome
905 maturation. mBio 5:e01874.

bioRxiv preprint doi: https://doi.org/10.1101/2025.02.14.638315; this version posted February 15, 2025. The copyright holder for this preprint (which was not certified by peer review) is the author/funder, who has granted bioRxiv a license to display the preprint in perpetuity. It is made available under aCC-BY-NC-ND 4.0 International license.

906 43. Cleary IA, Lazzell AL, Monteagudo C, Thomas DP, Saville SP. 2012. BRG1 and NRG1
907 form a novel feedback circuit regulating Candida albicans hypha formation and virulence.
908 Mol Microbiol 85:557-73.
909 44. Du H, Guan G, Xie J, Sun Y, Tong Y, Zhang L, Huang G. 2012. Roles of Candida
910 albicans Gat2, a GATA-type zinc finger transcription factor, in biofilm formation,
911 filamentous growth and virulence. PLoS One 7:e29707.
912 45. Thomas G, Bain JM, Budge S, Brown AJP, Ames RM. 2020. Identifying Candida
913 albicans Gene Networks Involved in Pathogenicity. Front Genet 11:375.
914 46. Lopes JP, Lionakis MS. 2022. Pathogenesis and virulence of Candida albicans. Virulence
915 13:89-121.
916 47. Ferrigno P, Posas F, Koepp D, Saito H, Silver PA. 1998. Regulated nucleo/cytoplasmic
917 exchange of HOG1 MAPK requires the importin beta homologs NMD5 and XPO1.
918 EMBO J 17:5606-14.
919 48. Polizotto RS, Cyert MS. 2001. Calcineurin-dependent nuclear import of the transcription
920 factor Crz1p requires Nmd5p. J Cell Biol 154:951-60.
921 49. Quan X, Rassadi R, Rabie B, Matusiewicz N, Stochaj U. 2004. Regulated nuclear
922 accumulation of the yeast hsp70 Ssa4p in ethanol-stressed cells is mediated by the N-
923 terminal domain, requires the nuclear carrier Nmd5p and protein kinase C. FASEB J
924 18:899-901.
925 50. Hall CJ, Boyle RH, Astin JW, Flores MV, Oehlers SH, Sanderson LE, Ellett F, Lieschke
926 GJ, Crosier KE, Crosier PS. 2013. Immunoresponsive gene 1 augments bactericidal
927 activity of macrophage-lineage cells by regulating beta-oxidation-dependent
928 mitochondrial ROS production. Cell Metab 18:265-78.

bioRxiv preprint doi: https://doi.org/10.1101/2025.02.14.638315; this version posted February 15, 2025. The copyright holder for this preprint (which was not certified by peer review) is the author/funder, who has granted bioRxiv a license to display the preprint in perpetuity. It is made available under aCC-BY-NC-ND 4.0 International license.

929 51. Scherer AK, Blair BA, Park J, Seman BG, Kelley JB, Wheeler RT. 2020. Redundant
930 Trojan horse and endothelial-circulatory mechanisms for host-mediated spread of
931 Candida albicans yeast. PLoS Pathog 16:e1008414.
932 52. Gervais NC, Halder V, Shapiro RS. 2021. A data library of Candida albicans functional
933 genomic screens. FEMS Yeast Res 21.
934 53. Witchley JN, Penumetcha P, Abon NV, Woolford CA, Mitchell AP, Noble SM. 2019.
935 Candida albicans Morphogenesis Programs Control the Balance between Gut
936 Commensalism and Invasive Infection. Cell Host Microbe 25:432-443 e6.
937 54. Brothers KM, Wheeler RT. 2012. Non-invasive imaging of disseminated candidiasis in
938 zebrafish larvae. J Vis Exp doi:10.3791/4051.
939 55. Bai C, Ramanan N, Wang YM, Wang Y. 2002. Spindle assembly checkpoint component
940 CaMad2p is indispensable for Candida albicans survival and virulence in mice. Mol
941 Microbiol 45:31-44.
942 56. Csank C, Schroppel K, Leberer E, Harcus D, Mohamed O, Meloche S, Thomas DY,
943 Whiteway M. 1998. Roles of the Candida albicans mitogen-activated protein kinase
944 homolog, Cek1p, in hyphal development and systemic candidiasis. Infect Immun
945 66:2713-21.
946 57. Davis D, Edwards JE, Jr., Mitchell AP, Ibrahim AS. 2000. Candida albicans RIM101 pH
947 response pathway is required for host-pathogen interactions. Infect Immun 68:5953-9.
948 58. Gratacap RL, Rawls JF, Wheeler RT. 2013. Mucosal candidiasis elicits NF-kappaB
949 activation, proinflammatory gene expression and localized neutrophilia in zebrafish. Dis
950 Model Mech 6:1260-70.

bioRxiv preprint doi: https://doi.org/10.1101/2025.02.14.638315; this version posted February 15, 2025. The copyright holder for this preprint (which was not certified by peer review) is the author/funder, who has granted bioRxiv a license to display the preprint in perpetuity. It is made available under aCC-BY-NC-ND 4.0 International license.

59. O'Meara TR, O'Meara MJ. 2021. DeORFanizing Candida albicans Genes using Coexpression. mSphere 6.

60. Castrejon F, Gomez A, Sanz M, Duran A, Roncero C. 2006. The RIM101 pathway contributes to yeast cell wall assembly and its function becomes essential in the absence of mitogen-activated protein kinase Slt2p. Eukaryot Cell 5:507-17.

61. Nobile CJ, Solis N, Myers CL, Fay AJ, Deneault JS, Nantel A, Mitchell AP, Filler SG. 2008. Candida albicans transcription factor Rim101 mediates pathogenic interactions through cell wall functions. Cell Microbiol 10:2180-96.

62. Petit J, Bailey EC, Wheeler RT, de Oliveira CAF, Forlenza M, Wiegertjes GF. 2019. Studies Into beta-Glucan Recognition in Fish Suggests a Key Role for the C-Type Lectin Pathway. Front Immunol 10:280.

63. Brenes LR, Lohse MB, Hartooni N, Johnson AD. 2020. A Set of Diverse Genes Influence the Frequency of White-Opaque Switching in Candida albicans. G3 (Bethesda) 10:2593-2600.

64. Enjalbert B, Smith DA, Cornell MJ, Alam I, Nicholls S, Brown AJ, Quinn J. 2006. Role of the Hog1 stress-activated protein kinase in the global transcriptional response to stress in the fungal pathogen Candida albicans. Mol Biol Cell 17:1018-32.

65. Kammer P, McNamara S, Wolf T, Conrad T, Allert S, Gerwien F, Hunniger K, Kurzai O, Guthke R, Hube B, Linde J, Brunke S. 2020. Survival Strategies of Pathogenic Candida Species in Human Blood Show Independent and Specific Adaptations. mBio 11.

66. Niemiec MJ, Grumaz C, Ermert D, Desel C, Shankar M, Lopes JP, Mills IG, Stevens P, Sohn K, Urban CF. 2017. Dual transcriptome of the immediate neutrophil and Candida albicans interplay. BMC Genomics 18:696.

bioRxiv preprint doi: https://doi.org/10.1101/2025.02.14.638315; this version posted February 15, 2025. The copyright holder for this preprint (which was not certified by peer review) is the author/funder, who has granted bioRxiv a license to display the preprint in perpetuity. It is made available under aCC-BY-NC-ND 4.0 International license.

67. Nobile CJ, Fox EP, Nett JE, Sorrells TR, Mitrovich QM, Hernday AD, Tuch BB, Andes DR, Johnson AD. 2012. A recently evolved transcriptional network controls biofilm development in Candida albicans. Cell 148:126-38.

68. Pountain AW, Collette JR, Farrell WM, Lorenz MC. 2021. Interactions of Both Pathogenic and Nonpathogenic CUG Clade Candida Species with Macrophages Share a Conserved Transcriptional Landscape. mBio 12:e0331721.

69. Wang JM, Woodruff AL, Dunn MJ, Fillinger RJ, Bennett RJ, Anderson MZ. 2021. Intraspecies Transcriptional Profiling Reveals Key Regulators of Candida albicans Pathogenic Traits. mBio 12.

70. Dalal CK, Zuleta IA, Mitchell KF, Andes DR, El-Samad H, Johnson AD. 2016. Transcriptional rewiring over evolutionary timescales changes quantitative and qualitative properties of gene expression. Elife 5.

71. Nocedal I, Mancera E, Johnson AD. 2017. Gene regulatory network plasticity predates a switch in function of a conserved transcription regulator. Elife 6.

72. Reuss O, Vik A, Kolter R, Morschhauser J. 2004. The SAT1 flipper, an optimized tool for gene disruption in Candida albicans. Gene 341:119-27.

73. Wu Y, Du S, Johnson JL, Tung HY, Landers CT, Liu Y, Seman BG, Wheeler RT, Costa-Mattioli M, Kheradmand F, Zheng H, Corry DB. 2019. Microglia and amyloid precursor protein coordinate control of transient Candida cerebritis with memory deficits. Nat Commun 10:58.

74. Moyes DL, Wilson D, Richardson JP, Mogavero S, Tang SX, Wernecke J, Hofs S, Gratacap RL, Robbins J, Runglall M, Murciano C, Blagojevic M, Thavaraj S, Forster TM, Hebecker B, Kasper L, Vizcay G, Iancu SI, Kichik N, Hader A, Kurzai O, Luo T,

bioRxiv preprint doi: https://doi.org/10.1101/2025.02.14.638315; this version posted February 15, 2025. The copyright holder for this preprint (which was not certified by peer review) is the author/funder, who has granted bioRxiv a license to display the preprint in perpetuity. It is made available under aCC-BY-NC-ND 4.0 International license.

997 Kruger T, Kniemeyer O, Cota E, Bader O, Wheeler RT, Gutsmann T, Hube B, Naglik JR.
998 2016. Candidalysin is a fungal peptide toxin critical for mucosal infection. Nature
999 532:64-8.
1000 75. Peters BM, Palmer GE, Nash AK, Lilly EA, Fidel PL, Jr., Noverr MC. 2014. Fungal
1001 morphogenetic pathways are required for the hallmark inflammatory response during
1002 Candida albicans vaginitis. Infect Immun 82:532-43.
1003 76. Seman BG, Moore JL, Scherer AK, Blair BA, Manandhar S, Jones JM, Wheeler RT.
1004 2018. Yeast and Filaments Have Specialized, Independent Activities in a Zebrafish
1005 Model of Candida albicans Infection. Infect Immun 86.
1006 77. Council NR. 2011. Guide for the care and use of laboratory animals. National Academies
1007 Press, Washington, D.C.
1008 78. Ellett F, Pase L, Hayman JW, Andrianopoulos A, Lieschke GJ. 2011. mpeg1 promoter
1009 transgenes direct macrophage-lineage expression in zebrafish. Blood 117:e49-56.
1010 79. Hall C, Flores MV, Storm T, Crosier K, Crosier P. 2007. The zebrafish lysozyme C
1011 promoter drives myeloid-specific expression in transgenic fish. BMC Dev Biol 7:42.
1012 80. de Oliveira S, Lopez-Munoz A, Martinez-Navarro FJ, Galindo-Villegas J, Mulero V,
1013 Calado A. 2015. Cxcl8-l1 and Cxcl8-l2 are required in the zebrafish defense against
1014 Salmonella Typhimurium. Dev Comp Immunol 49:44-8.
1015 81. Nguyen-Chi M, Laplace-Builhe B, Travnickova J, Luz-Crawford P, Tejedor G, Phan QT,
1016 Duroux-Richard I, Levraud JP, Kissa K, Lutfalla G, Jorgensen C, Djouad F. 2015.
1017 Identification of polarized macrophage subsets in zebrafish. Elife 4:e07288.

bioRxiv preprint doi: https://doi.org/10.1101/2025.02.14.638315; this version posted February 15, 2025. The copyright holder for this preprint (which was not certified by peer review) is the author/funder, who has granted bioRxiv a license to display the preprint in perpetuity. It is made available under aCC-BY-NC-ND 4.0 International license.

1018 82. Mattingly CJ, Hampton TH, Brothers KM, Griffin NE, Planchart A. 2009. Perturbation of
1019 defense pathways by low-dose arsenic exposure in zebrafish embryos. Environ Health
1020 Perspect 117:981-7.
1021 83. Quinn GP, Keough MJ. 2002. Experimental Design and Data Analysis for Biologists doi:
1022 https://doi.org/10.1017/CBO9780511806384 Cambridge University Press.
1023 84. Cohen J. 1988. Statistical Power Analysis for the Behavioral Sciences Routledge, New
1024 York.
1025 85. Hedges LV, Olkin O. 1985. Statistical Methods for Meta-Analysis. Academic Press.
1026

(which was not certified by peer review) is the author/funder, who has granted bioRxiv a license to display the preprint in perpetuity. It is made available under aCC-BY-NC-ND 4.0 International license.

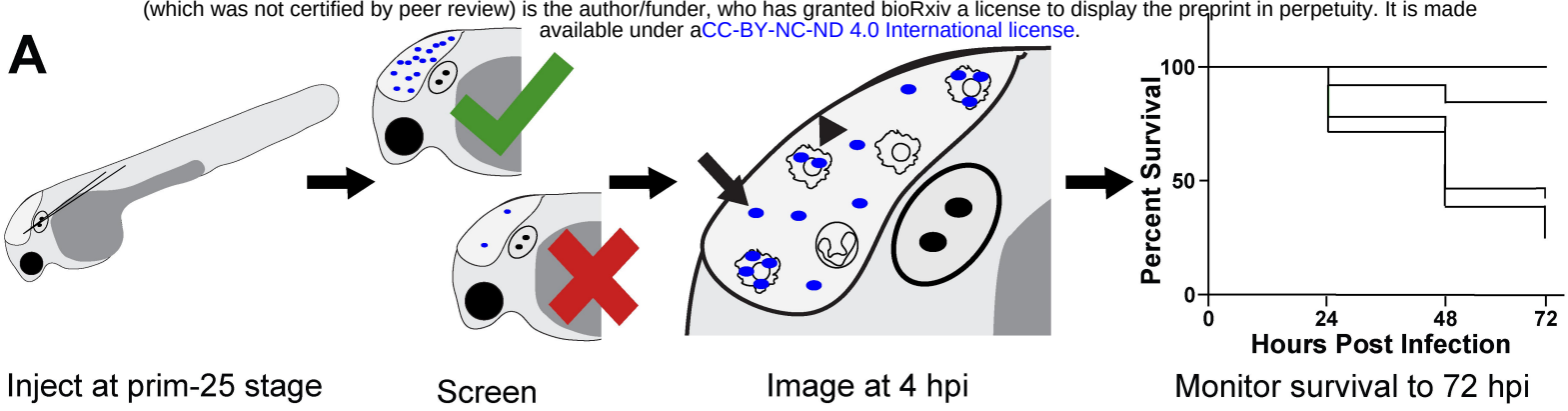

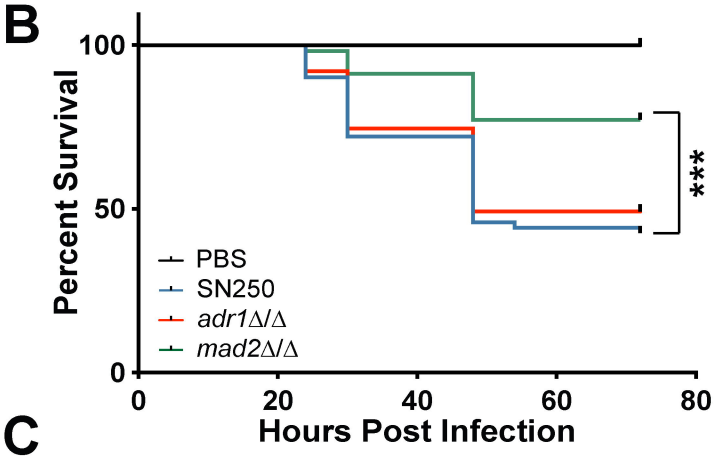

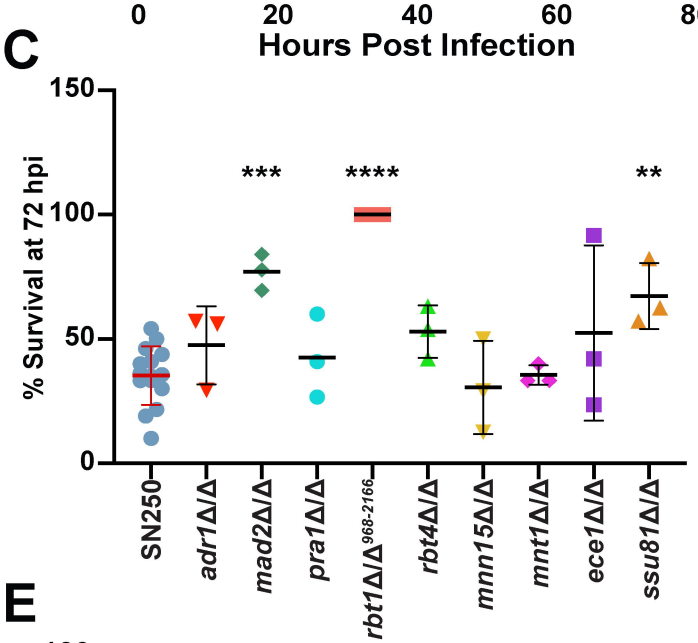

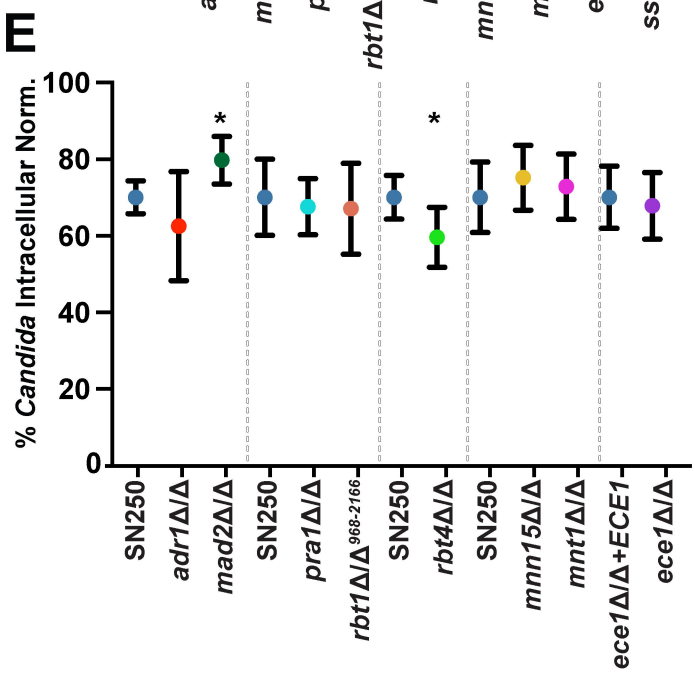

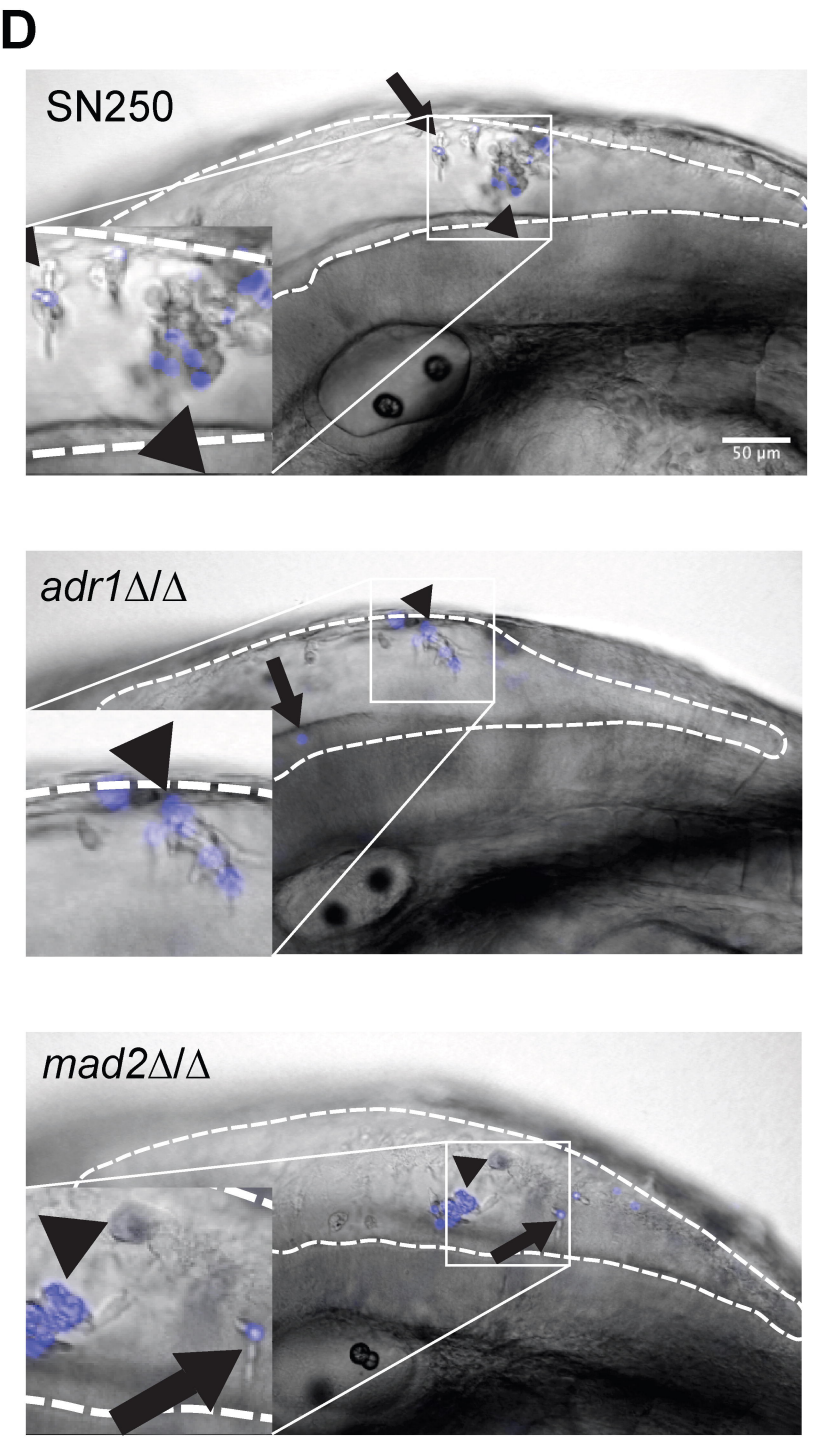

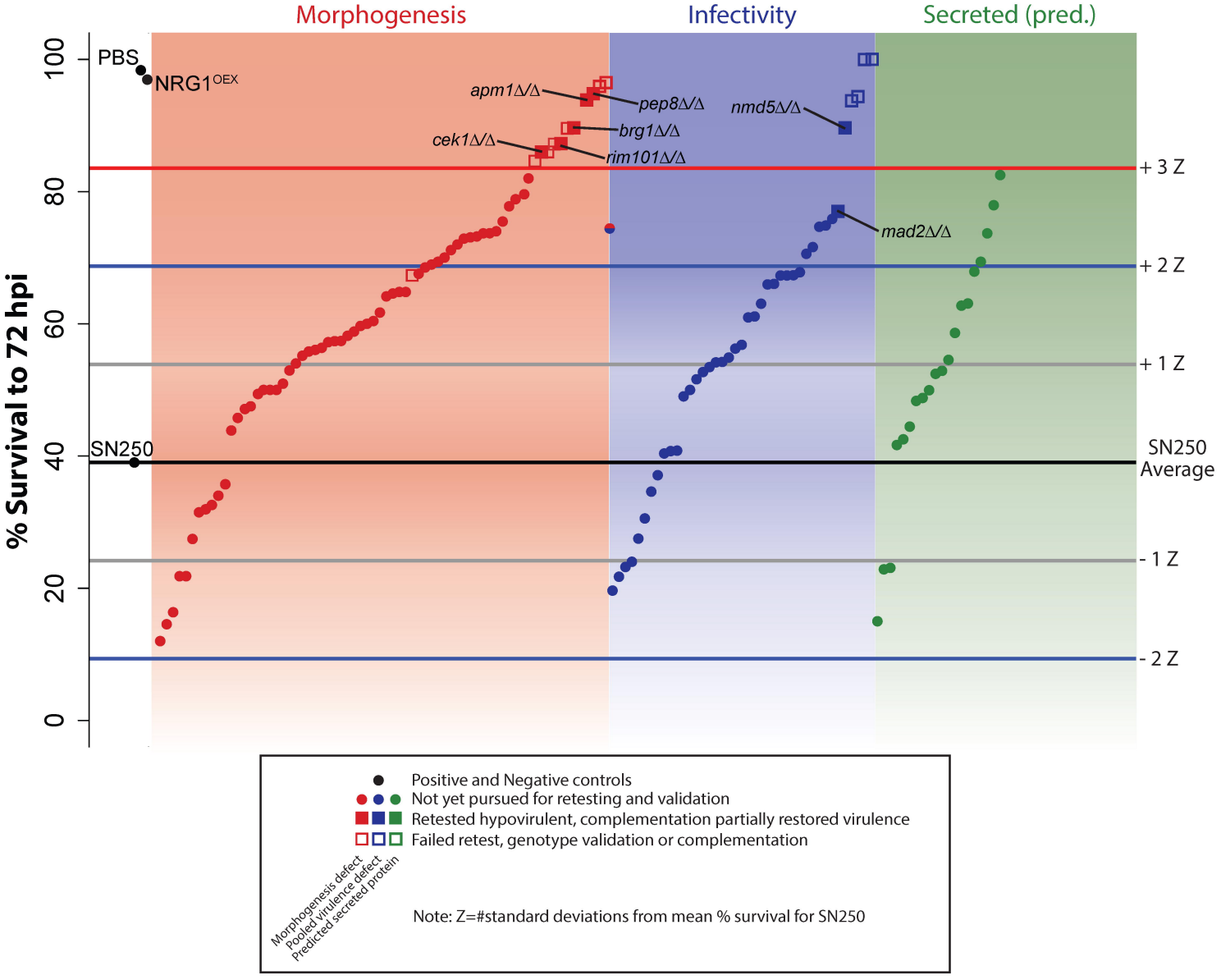
Morphogenesis
Infectivity
Secreted (pred.)
% Survival to 72 hpi
0
20
40
60
80
100
PBS
NRG1OEX
SN250
apm1Δ/Δ
pep8Δ/Δ
cek1Δ/Δ
brg1Δ/Δ
rim101Δ/Δ
nmd5Δ/Δ
mad2Δ/Δ
+ 3 Z
+ 2 Z
+ 1 Z
SN250 Average
- 1 Z
- 2 Z
Positive and Negative controls
Not yet pursued for retesting and validation
Retested hypovirulent, complementation partially restored virulence
Failed retest, genotype validation or complementation
Morphogenesis defect
Pooled virulence defect
Predicted secreted protein
Note: Z=#standard deviations from mean % survival for SN250

available under aCC-BY-NC-ND 4.0 International license.

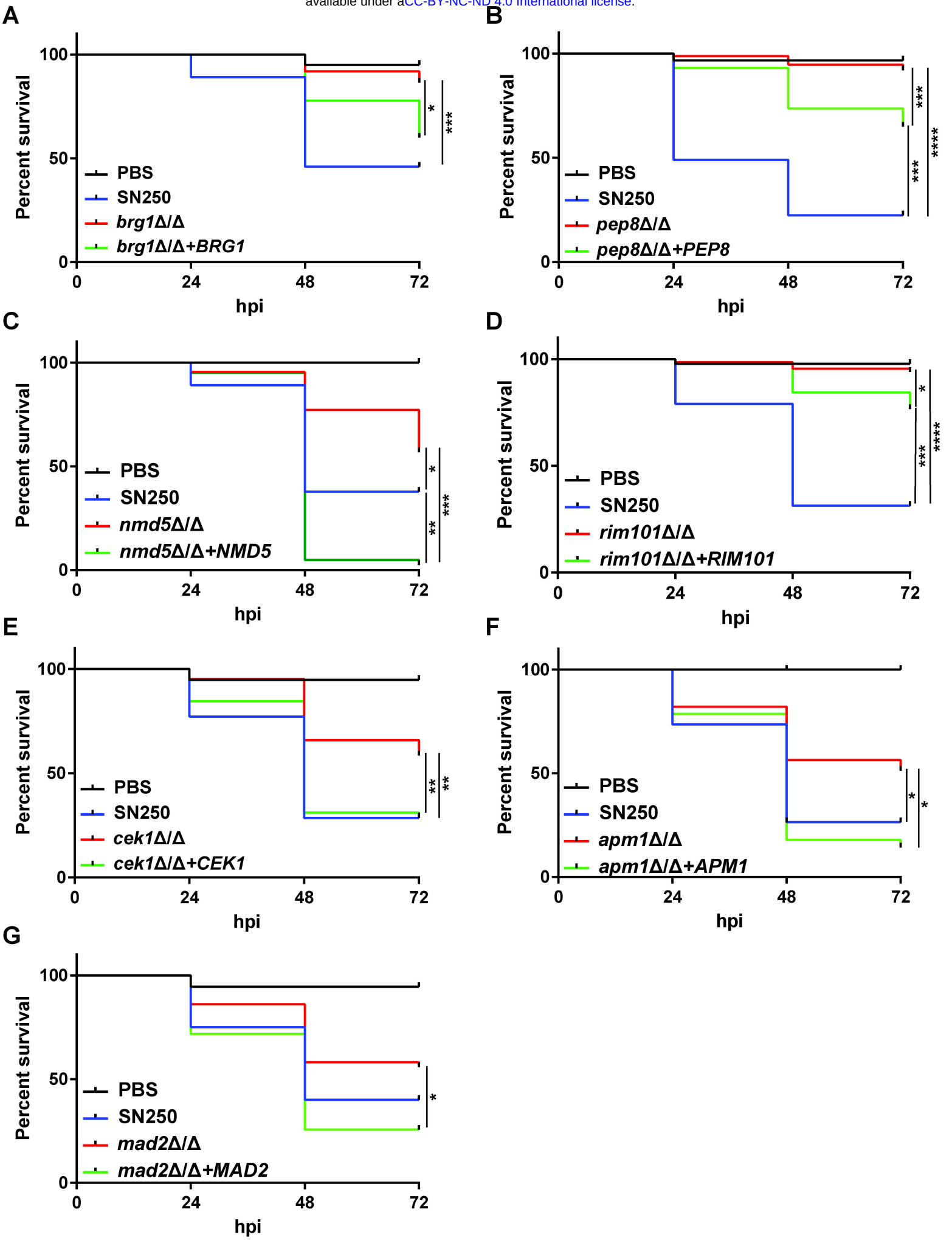

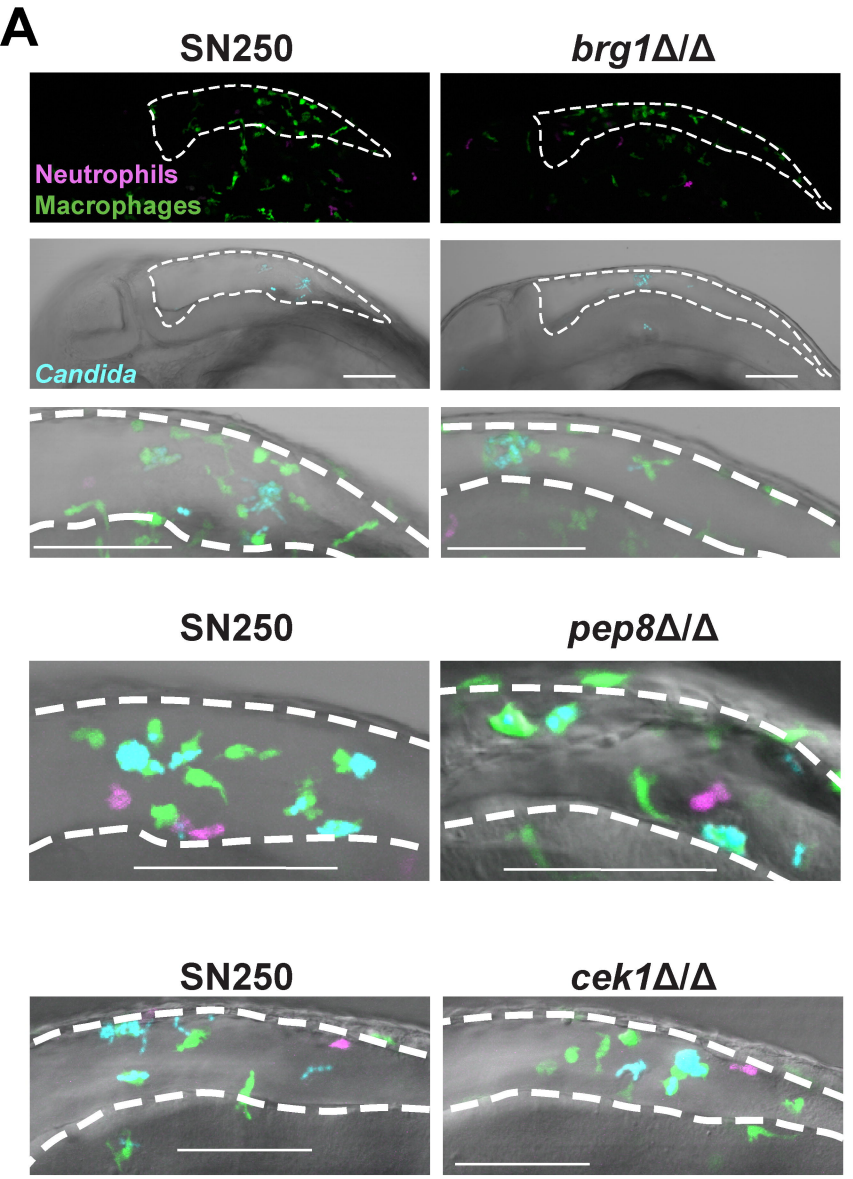

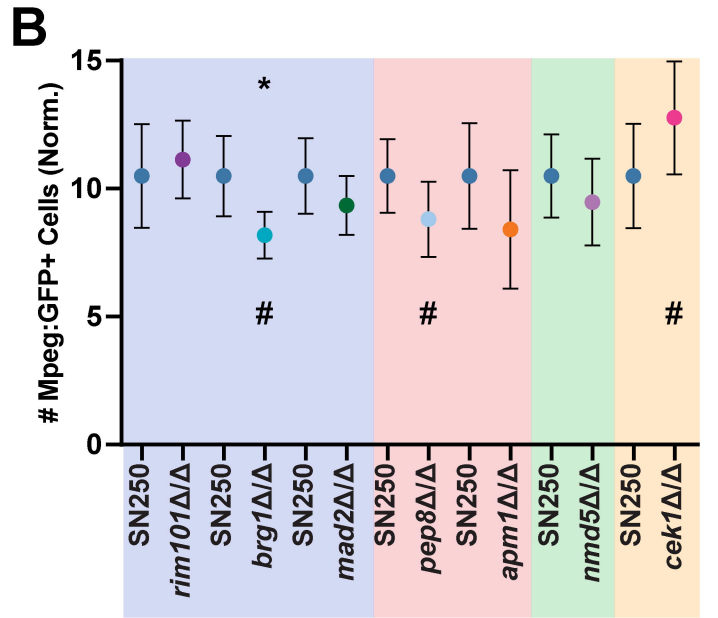

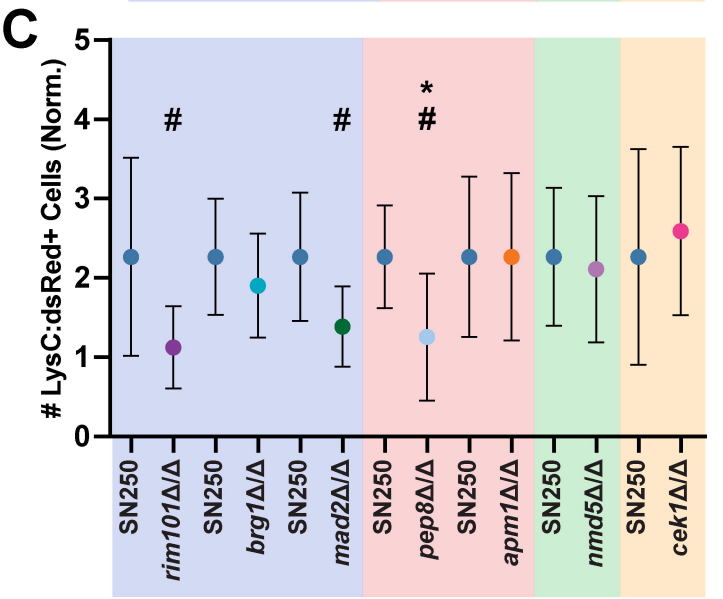

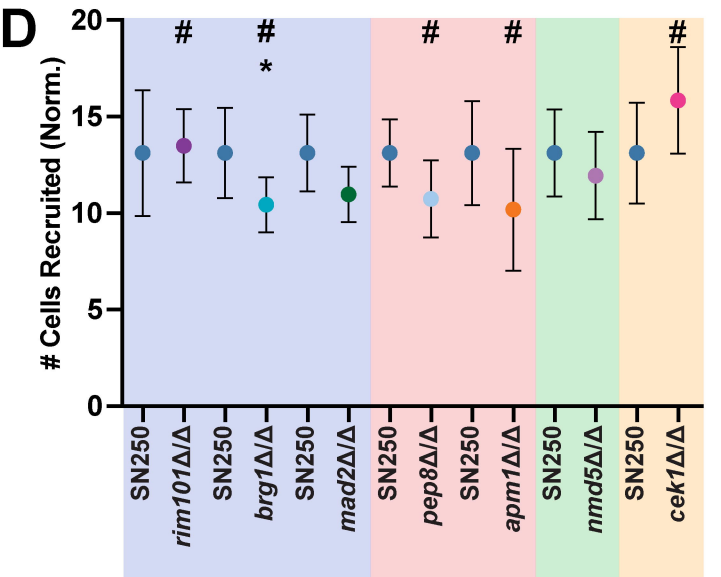

Key for panel A

Cell colors

Neutrophils
Macrophages
Candida

Hindbrain ventricle area

Key for panels B-D

Group I
Group II
Group III
Group IV

* p<0.05
\# moderate effect
\# large effect

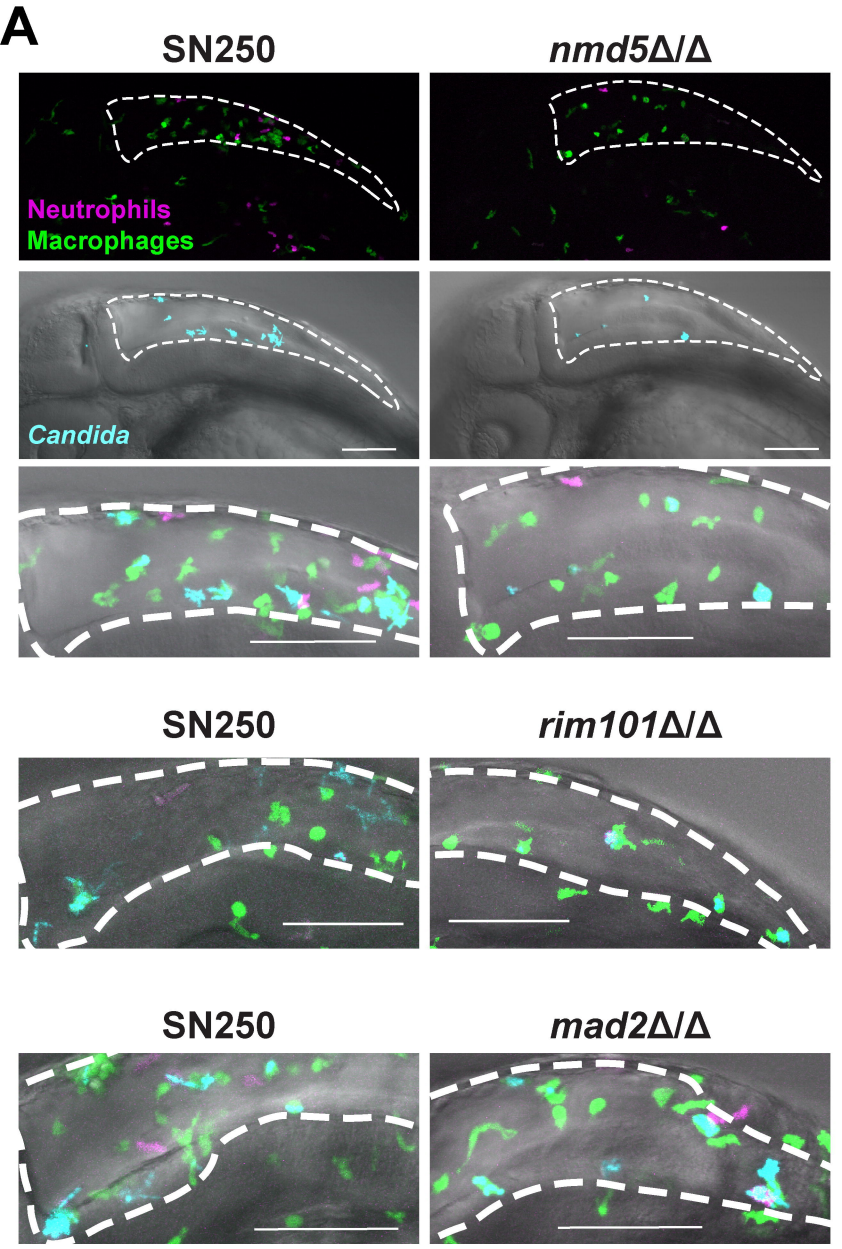

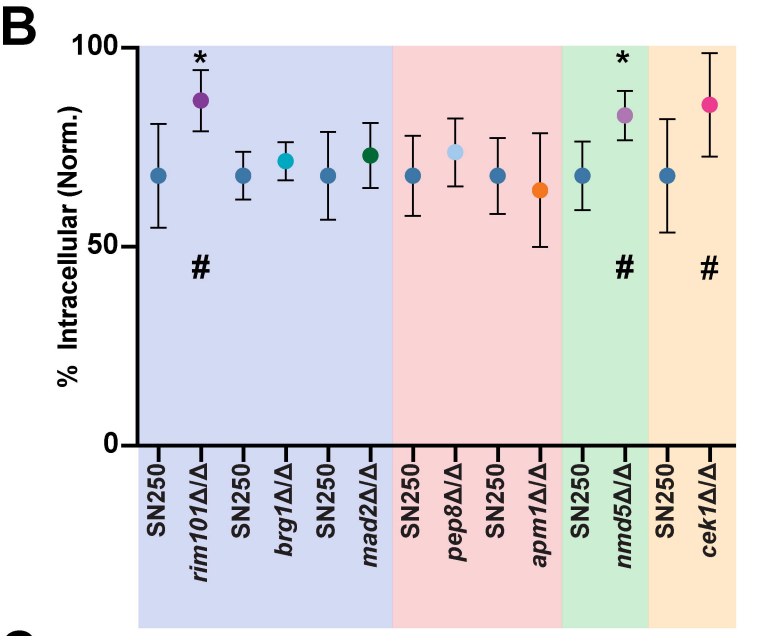

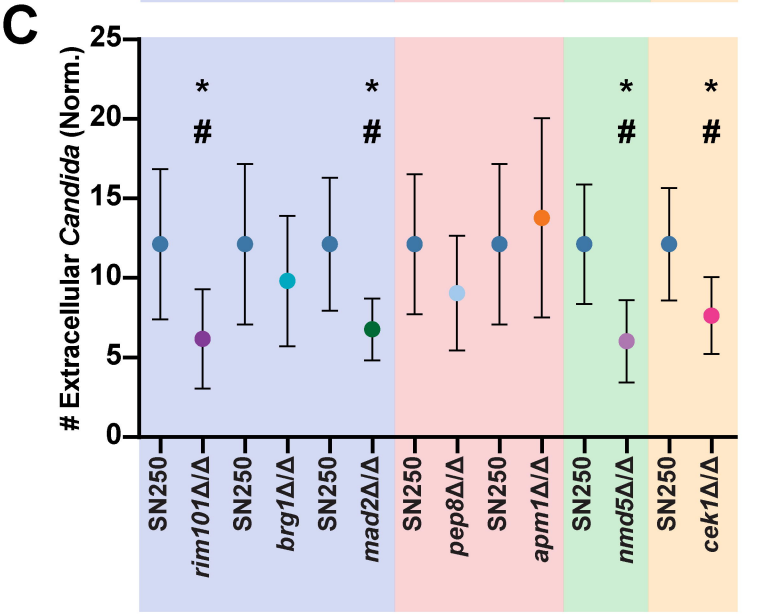

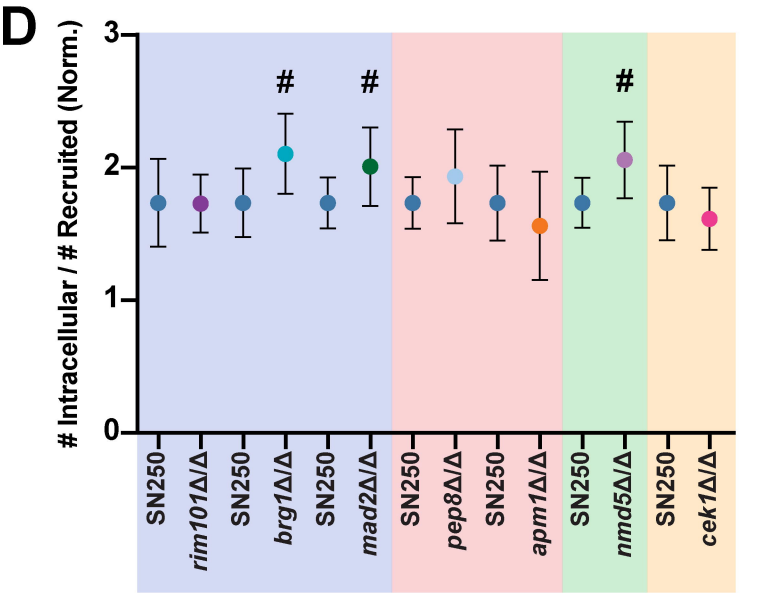

Key for panel A

Cell colors

Neutrophils
Macrophages
Candida

Hindbrain ventricle area

Key for panels B-D

Group I
Group II
Group III
Group IV

* p<0.05
# moderate effect
 # large effect

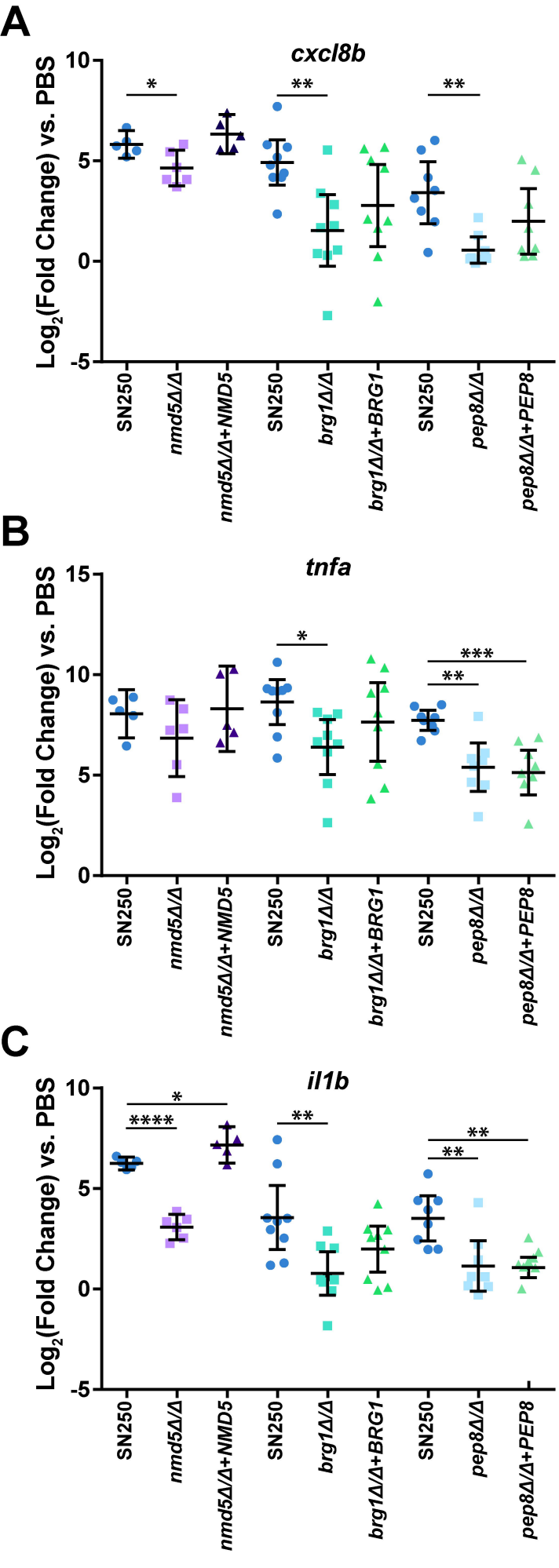
A
cxcl8b
Log2(Fold Change) vs. PBS
10
5
0
-5
*
**
**
SN250
nmd5Δ/Δ
nmd5Δ/Δ+NMD5
SN250
brg1Δ/Δ
brg1Δ/Δ+BRG1
SN250
pep8Δ/Δ
pep8Δ/Δ+PEP8
B
tnfa
Log2(Fold Change) vs. PBS
15
10
5
0
*
***
**
SN250
nmd5Δ/Δ
nmd5Δ/Δ+NMD5
SN250
brg1Δ/Δ
brg1Δ/Δ+BRG1
SN250
pep8Δ/Δ
pep8Δ/Δ+PEP8
C
il1b
Log2(Fold Change) vs. PBS
10
5
0
-5
*
****
**
**
**
SN250
nmd5Δ/Δ
nmd5Δ/Δ+NMD5
SN250
brg1Δ/Δ
brg1Δ/Δ+BRG1
SN250
pep8Δ/Δ
pep8Δ/Δ+PEP8

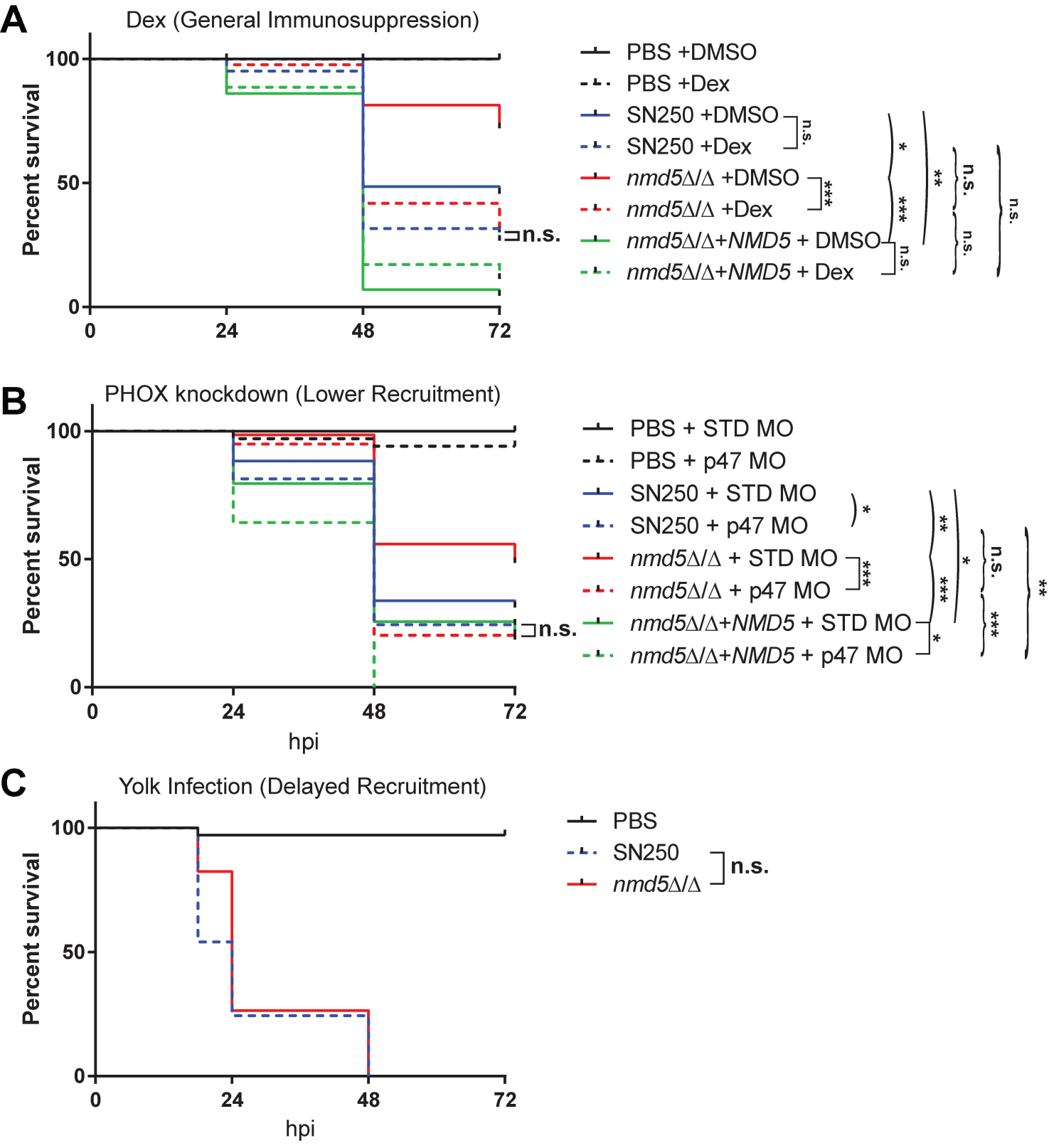
A
Dex (General Immunosuppression)
Percent survival
100
50
0
0
24
48
72
n.s.
PBS +DMSO
PBS +Dex
SN250 +DMSO
SN250 +Dex
nmd5Δ/Δ +DMSO
nmd5Δ/Δ +Dex
nmd5Δ/Δ+NMD5 + DMSO
nmd5Δ/Δ+NMD5 + Dex
n.s.
***
*
**
n.s.
n.s.
n.s.
B
PHOX knockdown (Lower Recruitment)
Percent survival
100
50
0
0
24
48
72
hpi
n.s.
PBS + STD MO
PBS + p47 MO
SN250 + STD MO
SN250 + p47 MO
nmd5Δ/Δ + STD MO
nmd5Δ/Δ + p47 MO
nmd5Δ/Δ+NMD5 + STD MO
nmd5Δ/Δ+NMD5 + p47 MO
*
***
**
*
n.s.
***
*
**
C
Yolk Infection (Delayed Recruitment)
Percent survival
100
50
0
0
24
48
72
hpi
PBS
SN250
nmd5Δ/Δ
n.s.